Ann. Rev. Astron. Astrophys. 1985. 23 : 19–57

FUNDAMENTAL AND APPLIED ASPECTS OF ASTRONOMICAL "SEEING"

C. E. Coulman

Cloud Physics Laboratory, Division of Atmospheric Research,
CSIRO, P. O. Box 134, Epping, N.S.W. 2121, Australia

1. PREFACE

Despite recent advances in the use of spacecraft as observatory platforms, much astronomy is still conducted from the surface of the Earth, as the existence of an IAU Commission on Site Identification and Protection testifies.

The literature on astronomical seeing and observatory site selection is widely scattered throughout journals and conference reports concerned with astronomy, pure and applied optics, radio science, and meteorology, with the occasional relevant chapter in astronomy textbooks; site surveys are often recorded in the internal reports of institutions. Although reviews of various aspects of the subject have appeared from time to time, it seems appropriate to provide an account of the subject with the particular needs of practicing astronomers in mind. This review aims to represent the state of the subject up to 1982, covering the pure and applied facets of both the optical and meteorological aspects.

Each section has the same overall structure: a general description is accompanied by a more detailed, and in some cases mathematical, treatment of essential aspects of the matter under discussion. The extensive bibliography facilitates access to the literature for those seeking further specialized information.

2. HISTORY AND PROSPECTS

In the recorded history of phenomena that we now describe by the term atmospheric "seeing," one of the earliest references was made by Aristotle to

0066–4146/85/0915–0019$02.00

stellar scintillation in his treatise on "The Heavens" (95). In the Middle Ages, Roger Bacon (42) interested himself in the twinkling of stars, and during the Renaissance in Europe the fluctuating appearance of stars and planets became the concern of many workers engaged in astronomy with the recently invented telescope. Newton (203) recognized that his observations were often limited by the fact that that "the air through which we look is in perpetual tremor," and he speculated on the best kinds of sites for observatories: "The only Remedy is a most serene and quiet Air, such as may perhaps be found on the tops of the highest Mountains above the grosser Clouds." With modern Earth-based astronomical instruments, it is still predominantly the image-transmitting properties of the atmosphere that limit performance to a level usually well below that of which the instruments are theoretically capable (see, for example, 62, 67, 200, 223, 229). However, means are being developed for reducing the image-degrading effects of seeing (Section 6).

Although observations of the effects of seeing date from ancient times, it is only comparatively recently that progress has been made in understanding the phenomenon. Aristotle's interpretation of what he saw was based on the belief that sight depended on rays issuing from the eye of the viewer. Roger Bacon offered a physiological explanation for the scintillation of stars, and it seems to have been Tycho Brahe (202) who first postulated a partly atmospheric cause for this phenomenon. Kepler (202) preferred to believe that the light from Venus fluctuated at source when, in 1602, he made his observations of "shadow bands" on a white wall illuminated by the planet. Robert Hooke (134) first suggested the existence of "small, moving regions of atmosphere having different refracting powers which act like lenses" and thus introduced the refraction theory of scintillation.

Advances in the selection and evaluation of observatory sites followed from the development of the semiquantitative visual scale of seeing proposed by Danjon (81), the photography of star trails by Couder (55), and the photoelectric detection of scintillation by Whitford & Stebbins (268). In the last 25 years, site testing has embodied both optical and meteorological observations: examples are the surveys that led to the choice of Kitt Peak (USA) and Cerro Tololo (Chile) [briefly described by Stock & Keller (237)] and the comprehensive optical and meteorological survey planned by Coulman (60) for the Smithsonian Institution Observatory at Mount Hopkins, Arizona, with the observations carried out by Pearlman et al. (208, 209).

One of the most comprehensive site selection programs yet envisaged is that of the Joint Organization for Solar Observations (JOSO), founded in 1969 to coordinate European interests in locating an excellent solar observatory site (85). Some of the JOSO work centered on the Canary

Islands, and more recently a program relating to night seeing conditions there has been undertaken by the Royal Greenwich Observatory (248, 249) and the Royal Observatory of Edinburgh.

The present article is concerned with both optical and meteorological work of the past two or three decades that is directly applicable to atmospheric seeing. Some overlap with other reviews is, of course, inevitable in the interests of completeness—e.g. with reviews of research on scintillation (140, 185) and on many aspects of the effects of turbulence on imagery from the standpoint of optical physics (223). Recent developments in high-resolution image processing have also been reviewed (269).

The prospects for improvements in the image quality received at optical observatories appear to lie in two main directions. On the one hand, advances in our basic understanding of atmospheric seeing should continue to improve site-selection procedures and also improve the conditions at existing observatories by reducing the local effects of seeing in the immediate vicinity of telescopes and domes. On the other hand, new techniques exist for separating useful signal from unwanted noise, and telescopes can be provided with a dynamic capability to correct for some of the image degradation attributable to the atmosphere.

Existing microthermal techniques and recent methods of analyzing seeing-monitor records provide adequate measurements of the sources of bad seeing, but the major outstanding problem is to relate seeing quality causally to larger-scale meteorological factors. Until this can be achieved, site testing will remain a statistical exercise involving observations conducted over many seasons.

3. THE OPTICS OF "SEEING"

When an electromagnetic wave of uniform amplitude is launched into a refractively nonuniform medium, some of the energy of the wave is scattered by the refractive inhomogeneities, and as the wave propagates it exhibits amplitude and phase fluctuations. Consequently, an optical image formed by focusing such a wave exhibits fluctuations in *intensity*, *sharpness*, and *position*, which we refer to as *scintillation*, *image blurring*, and *image movement*, respectively.

3.1 *Résumé of the Theory of Wave Propagation in a Turbulent Atmosphere*

In the theory of image propagation, we have to address ourselves to two main problems: (*a*) the calculation of amplitude and phase statistics of the wave after propagation for a known distance; and (*b*) the specification of image quality after a sample of the wave front has been collected by a

telescope. Later in this review we utilize some relationships derived from the theory of optical propagation (243) to discuss applications to astronomy. Further improvements by Tatarski (244), Clifford et al. (49), Tatarski et al. (245), and Dashen (83) have extended the theory to account for additional phenomena, such as the asymptotic approach of scintillation to a saturation limit (113). The status of propagation theory has been well reviewed (11), and it is worth noting that earlier idealized but unrealistic representations (see, for example, 23, 167, 217) have been superseded. However, Lee & Harp (163) revived the "phase screen" approach, which is largely used in Roddier's review (223).

3.1.1 PLANE-WAVE PROPAGATION We consider the propagation of plane waves in a turbulent, transparent medium of refractive index N, which is only a function of position $\mathbf{r}$. The finest structure (represented by l_0) in the field of N is assumed large compared with the wavelength λ. For the atmosphere, we have

$$N(\mathbf{r}) = 1 + N_1(\mathbf{r}), \tag{3.1}$$

where

$$N_1(\mathbf{r}) \ll 1. \tag{3.2}$$

The time-independent, scalar wave equation may be written as

$$\nabla^2 u + \left(\frac{2\pi}{\lambda}\right)^2 N^2(\mathbf{r}) u = 0, \tag{3.3}$$

where, for a plane wave of amplitude $\mathscr{A}$ and phase S, we put

$$u = \mathscr{A} \exp(iS). \tag{3.4}$$

If the wave exhibits only *small perturbations*, we may find a solution of Equation 3.3 in the form of an unperturbed wave u_0 and a perturbation u_1, where $|u_0| \gg |u_1|$. The fluctuations of logarithmic-amplitude and phase may be expressed as

$$\ln\left(\frac{\mathscr{A}}{\mathscr{A}_0}\right) = \mathrm{Re}\left[\frac{u_1}{u_0}\right] = \chi \tag{3.5}$$

and

$$S - S_0 = \mathrm{Im}\left[\frac{u_1}{u_0}\right] = S_1. \tag{3.6}$$

Here $\mathscr{A}_0$ and S_0 are the amplitude and phase of u_0. Chernov (46) and Tatarski (243) used a transformation, ascribed to Rytov (230), that permits a solution of Equation 3.3 under less restrictive conditions. The wave

equation is cast in the form

$$\frac{\nabla^2 u}{u} + \left(\frac{2\pi}{\lambda}\right)^2 N^2(\mathbf{r}) = \nabla^2 \ln u + (\nabla \ln u)^2 + \left(\frac{2\pi}{\lambda}\right)^2 N^2(\mathbf{r}) = 0, \qquad 3.7$$

which, since it contains only *derivatives* of $\ln u$, may be solved for *smooth perturbations*. Expressions similar to Equations 3.5 and 3.6 for the log-amplitude and phase fluctuations are obtained.

For a plane wave propagating along a direction x in a nonuniform medium, the statistics of fluctuations of amplitude and phase in a plane x = constant may be related to corresponding statistics of refractive index fluctuations. Tatarski (243) expanded the refractive index field in spectral form in Cartesian coordinates x, y, and z as

$$N_1(x, y, z) = N_1(x, 0, 0) + \int_{-\infty}^{\infty}\int [1 - \exp\, i(\kappa_2 y + \kappa_3 z)]\, dZ(\kappa_2, \kappa_3, x), \qquad 3.8$$

where $dZ(\kappa_2, \kappa_3, x)$ denotes the spectral amplitudes of the random field of N_1 for wave numbers κ_2, κ_3. After substitution in the wave equation, we obtain a solution that relates the spectrum of fluctuations of the wave field to that of the refractive index field. The spectral density function F_S is related to the structure function[1] $D_S(r)$ by

$$D_S(r) = 4\pi \int_0^{\infty} [1 - J_0(\kappa r)] F_S(\kappa, 0) \kappa\, d\kappa, \qquad 3.9$$

and similarly for $D_{\mathscr{S}}(r)$; J_0 is the zero-order Bessel function.

For locally isotropic turbulent fields, Kolmogorov (151) has shown that the one-dimensional structure function has the form

$$D_N(r) = C_N^2 r^{2/3}, \qquad 3.10$$

where C_N^2 is called the refractive index structure coefficient. The corresponding spectral function is written as

$$F_N(\kappa) = \text{constant}\ (C_N^2 \kappa^{-5/3}). \qquad 3.11$$

Further discussion of the restrictions of local isotropy and the extension to three-dimensional spectra is given in Yaglom (275), and the meteorological

[1] In one dimension x, a structure function for the variable S is defined as

$$D_S(r) = \langle [S(x+r) - S(x)]^2 \rangle,$$

where the angle brackets denote an average. It represents a mean squared fluctuation over a span r along the direction x.

implications are discussed in Section 4 of this article. It follows from Equations 3.9 and 3.11 that if $r \gtrsim (\lambda x_1)^{1/2}$, where x_1 is the propagation distance, then

$$D_{\mathscr{A}}(r) + D_S(r) = D_W(r) = 2.91 \left(\frac{2\pi}{\lambda}\right)^2 x_1 C_N^2 r^{5/3}, \quad 3.12$$

where $D_W(r)$ is called the wave structure function. In general C_N varies along the propagation path, and Equation 3.12 becomes

$$D_W(r) = 2.91 \left(\frac{2\pi}{\lambda}\right)^2 r^{5/3} \int_0^{x_1} C_N^2(x)\, dx. \quad 3.13$$

3.1.2 RANGE OF VALIDITY OF PROPAGATION THEORY The simplest treatment of wave propagation (the geometrical optics method) neglects the effects of diffraction entirely. For these effects to be negligible, we must have

$$x_1 < \frac{l_0^2}{\lambda}. \quad 3.14$$

For realistic values ($\lambda = 0.5\ \mu$m, $l_0 \approx 1$ mm) we find $x_1 \not> 2$ m. Such a short path length is of no practical interest in astronomy, and so we have not used the geometrical optics approximation.

Equations 3.5 and 3.6 are subject to the conditions $|\chi| \ll 1$ and $|S_1| \ll 1$, and Equation 3.7 involves the restrictions $\lambda|\nabla\chi| \ll 1$ and $\lambda|\nabla S_1| \ll 2\pi$. There has been much discussion about the relative severity of these restrictions (e.g. 48, 86, 239, 240); Tatarski (244) argued that Equation 3.7 implies the restriction

$$x_1 < \frac{l_0^4}{\lambda^3}, \quad 3.15$$

which for realistic values of l_0 and λ permits x_1 to exceed 10 km.

3.1.3 IMAGE-QUALITY ASSESSMENT From among the many methods available for specifying image quality, three are widely used in astronomy:

1. Image dimensions
2. Optical transfer function (OTF)
3. Strehl definition.

The modulation transfer function MTF (or modulus of the complex OTF) is a measure of the contrast reduction suffered by each Fourier component (spatial frequency) of the object after transmission through the entire imaging system. Fluctuations in the argument of the OTF indicate changes in the position and symmetry of the point image in the focal plane.

A formal treatment is given by Born & Wolf (26), a simpler discussion by Smith (233), and a nonmathematical, diagrammatic description by Perrin (212, 213).

The elementary incoherent object is a self-luminous point, and the elementary image is the spread-function $s(\eta, \zeta)$ in the image plane at $x = \xi$. For spatial frequencies f_η, f_ζ, the OTF is given by

$$A(f_\eta, f_\zeta) \propto \int_{-\infty}^{\infty}\int s(\eta, \zeta) \exp[-2\pi i(f_\eta \eta + f_\zeta \zeta)]\, d\eta\, d\zeta, \qquad 3.16$$

and f_η in the image plane is related to correlation distance r_η in the pupil plane by

$$f_\eta = \frac{r_\eta}{\lambda F} = \frac{y - y'}{\lambda F} \qquad 3.17$$

for imagery by a thin lens of focal length F.

Hufnagel & Stanley (137) showed that when the image integration time t' is longer than the period of the lowest-frequency image fluctuation, the average OTF is given by the average of its modulus (denoted by M). Thus, in one dimension,

$$\begin{aligned} \langle M(f)\rangle_{t'} &= A(f)\langle M(\lambda F f, x_1)\rangle_{t'} \\ &= A(f) \exp[-\tfrac{1}{2}D_W(r)], \end{aligned} \qquad 3.18$$

where $t' \to \infty$, $D_W(r)$ is given by an equation such as Equation 3.13, the angle brackets denote an average, and $A(f)$ is the time-independent MTF of the telescope. Trabka (251) and Fried (101) obtained identical results by different methods.

The effects of reducing averaging time toward the limit of the instantaneous image have been discussed, for example, by Coulman (57, 58, 61) and Fried (101), who showed that when the image integration time is short enough for the MTF to be unaffected by first-order tilts of the wave front (i.e. when the effects of image movement are removed), Equation 3.18 becomes

$$\langle M(f)\rangle_{t' \neq \infty} = A(f) \exp\left[-\frac{1}{2}D_W(r)\left\{1 - \frac{1}{b}\left(\frac{\lambda F f}{r_L}\right)^{1/3}\right\}\right], \qquad 3.19$$

with $b = 1$ for the near field, $b = 2$ for the far field, and r_L the diameter of the telescope. The validity of this analysis was supported by experiments (61); more recent contributions are reviewed by Roddier (223).

The Strehl definition may be used as a "figure of merit" for a system

whose MTF is known; it is given by

$$\mathscr{S} = \frac{\int_{-\infty}^{\infty} M(\mathbf{f})\, d\mathbf{f}}{\int_{-\infty}^{\infty} M_o(\mathbf{f})\, d\mathbf{f}}, \qquad 3.20$$

where subscript "o" denotes a diffraction-limited optical system and **f** is a vector spatial frequency in the image plane. It is generally accepted that images for which $\mathscr{S} \geqslant 0.8$ are not noticeably degraded (166).

3.1.4 THE WAVELENGTH DEPENDENCE OF SEEING Since the wave-structure function given in Equation 3.13 is wavelength dependent, it is of interest to determine whether seeing effects can be minimized by selection of particular regions of the optical spectrum for making observations.

Fried (101) chose to use a measure of resolution $\mathscr{R}$, defined as

$$\mathscr{R} = \int_{-\infty}^{\infty} M(\mathbf{f})\, d\mathbf{f}, \qquad 3.21$$

and showed that its maximum $\mathscr{R}_{max}$ could be written as

$$\mathscr{R}_{max} = \frac{\pi}{4}\left(\frac{r_0}{\lambda F}\right)^2, \qquad 3.22$$

where r_0 is used to normalize the parameter r in Equation 3.13 and is defined by

$$D_w(r) = \text{constant} \times (r/r_0)^{5/3}. \qquad 3.23$$

The parameter r_0 is a function of the integral in Equation 3.13 and is therefore a measure of atmospheric seeing quality, which varies as

$$r_0 \propto \lambda^{6/5}; \qquad 3.24$$

thus as λ increases, the ratio r_L/r_0 decreases slowly. Hence for a given telescope diameter r_L, we slowly approach diffraction-limited imagery as wavelength is increased by improving the match between telescope size and atmospheric limitations. The improvement is not very marked, as Young (278) argued, but Brown (33) considers it worthwhile for telescopes of more than 1 m in diameter operating at wavelengths longer than 2 μm.

4. THE METEOROLOGY OF "SEEING"

Image degradation is mainly attributable to turbulence on scales that are very small by meteorological standards, and the literature directly con-

cerned with seeing contains many references to turbulence studies (e.g. 53, 151, 192, 193, 246). Nevertheless, if we are seeking generally applicable methods of discussing and predicting seeing quality, we need to establish relationships between readily observable bulk properties of the atmosphere and the small-scale turbulent structure.

Although both turbulent and laminar motions are observed in the atmosphere (17), with the latter sometimes giving rise to low-frequency image wandering, it is evident from Sections 3 and 5 that seeing can be largely treated in terms of the intensity of turbulent refractive inhomogeneity.

4.1 *Micrometeorology and Small-Scale Turbulence Near the Surface*

4.1.1 SMALL-SCALE TURBULENCE The surface boundary layer can exhibit strong turbulent fluctuations of refractive index, particularly during the day-time when it is unstably stratified. There are various reference works on this widely studied regime (e.g. 107, 130, 172, 192, 193, 198, 214, 241). In studying the eddy transfer process in turbulence, Kolmogorov (151) proposed two important hypotheses.

The first suggests that the spectral density function of the velocity field in locally isotropic turbulence depends only on the dissipation rate ε, the viscosity ν, and of course the spatial wave number κ.

The second suggests that for a range of wave numbers, the spectral density function is independent of ν. In the range of the second hypothesis, called the "inertial interval," the structure function $D_v(r)$ (Section 3.1.1) has the form

$$D_v(r) \propto (r\varepsilon)^{2/3} = C_v^2 r^{2/3}, \qquad 4.1$$

which is known as Kolmogorov's Law; C_v^2 is called the velocity structure coefficient (or sometimes, the structure constant).

Similar expressions hold for any "passive additive" variable; for example, the structure function for temperature is given by

$$D_T(r) = C_T^2 r^{2/3}, \qquad 4.2$$

and it follows that the one-dimensional spectral density function has the form (53, 275)

$$F_T(\kappa) \propto (\kappa)^{-5/3}. \qquad 4.3$$

Despite restriction to locally homogeneous random fields, this theory has facilitated the interpretation of observed data that cannot always be shown to conform precisely to such ideals. A further practical requirement is the facility to interchange spatial and temporal scales. Taylor (246 hy-

pothesized that the general form of a turbulent field is conserved as the perturbations are carried along by the mean flow. Hence, a spatial span r is convertible to a time interval t' by

$$r = Ut', \tag{4.4}$$

where U is the mean speed along the axis of r. Much evidence has been accumulated in favor of this hypothesis (172, 191).

4.1.2 TURBULENT FLUCTUATIONS OF REFRACTIVE INDEX A small fluctuation dN may be expressed as

$$dN = \frac{\partial N}{\partial T}\,dT + \frac{\partial N}{\partial e}\,de + \frac{\partial N}{\partial p}\,dp, \tag{4.5}$$

as noted by Bean & Dutton (20) and Wesely (266), where p is the atmospheric pressure and e the water vapor partial pressure. Hence, we have

$$C_N^2 = C_T^2 + 2aC_{Tq} + a^2C_q^2 \tag{4.6}$$

(see 274), where C_{Tq} is a coefficient referring to the covariance structure of temperature and humidity, q is the water vapor mixing ratio, and a is a constant. Observations by Friehe et al. (105), Antonia et al. (6), Wesely & Hicks (267), and Coulman (69) have shown that the effects of humidity can be significant for horizontal propagation in a marine boundary layer. However, for most astronomical purposes, we have

$$C_N^2 = \left[\frac{8 \times 10^{-5}\,p}{T^2}\right]^2 C_T^2, \tag{4.7}$$

where T is in degrees Kelvin and p is in millibars.

4.1.3 STRATIFICATION IN THE LOWER ATMOSPHERE Turbulent motion is generated partly by airflow over rough surfaces, partly by wind shear in free air, and partly by buoyancy forces. The rate of generation of kinetic energy of turbulence per unit mass is

$$TKE = \frac{\tau}{\rho}\cdot\frac{\partial U}{\partial z} + \frac{gH}{c_p\rho\theta_v}, \tag{4.8}$$

where g is gravitational acceleration, θ_v the virtual potential temperature,[2] U the horizontal wind speed, τ the vertical momentum flux, H the heat flux, c_p the specific heat of air at constant pressure, and ρ the air density.

[2] Potential temperature θ is defined for temperature T (K) and pressure p (mbar) as $\theta = T(p/1000)^{-0.288}$. It is inversely proportional to the density of dry air, while θ_v includes the effect of water vapor on density and so is given by $\theta_v = \theta(1 + 0.61 \times 10^{-3}\,q)$.

Equilibrium with respect to buoyancy forces is stable, neutral, or unstable depending on whether

$$\frac{\partial \theta_v}{\partial z} > 0, \qquad \frac{\partial \theta_v}{\partial z} = 0, \quad \text{or} \quad \frac{\partial \theta_v}{\partial z} < 0. \tag{4.9}$$

Thus the wind-generated turbulence is augmented by buoyancy in unstable, convective situations and is suppressed in stable conditions. The degree of stability is measured by the flux Richardson number R_f,

$$R_f = \frac{-gH}{c_p \theta_v \tau(\partial U/\partial z)}, \tag{4.10}$$

the gradient Richardson number R_i,

$$R_i = \frac{g}{\theta_v} \frac{(\partial \theta_v/\partial z)}{(\partial U/\partial z)^2}, \tag{4.11}$$

or by a quantity L, having dimensions of length, defined by Obukhov (205) as

$$L = \frac{-u_*^3 c_p \rho \theta}{kgH}. \tag{4.12}$$

Here u_* is called the friction velocity.

Simple mixing-length theory (241) shows that in neutral stability, with von Kármán's constant $k \simeq 0.4$,

$$U(z) = \frac{u_*}{k} \ln\left(\frac{z}{z_0}\right), \tag{4.13}$$

where z_0 is called the "roughness length" and is the height at which $U \to 0$. It characterizes the aerodynamic roughness of the surface. A similar but more elaborate formulation extends to the case of nonneutral stratification, as given in Haugen (130).

The vertical variation of the properties of the lower atmosphere may conveniently be expressed in terms of a normalized height z/L, and practical ways of obtaining the L-value in a variety of conditions are well described in Webb (265).

4.1.4 UNSTABLE STRATIFICATION A schematic representation of stratification in the lower troposphere is shown in Figure 1; the planetary boundary layer may be idealized as a three-layer structure, with a gradual transition of properties between layers. The characteristics of these layers are as follows:

1. The surface boundary layer, where shear is the dominant source of

turbulence, has a normalized depth $z/|L| \approx 0.03$, a virtual potential temperature gradient $\partial\theta_v/\partial z \propto z^{-1}$, and $C_T^2 \propto z^{-2/3}$.

2. The free convection layer, where the actual height z above the surface is the significant length scale, has a depth $z/|L| \approx 1$, a virtual potential temperature gradient $\partial\theta_v/\partial z \propto z^{-4/3}$, and $C_T^2 \propto z^{-4/3}$.
3. The third layer is usually well mixed by convection, has a vanishingly small gradient $\partial\theta_v/\partial z$, and is topped by an inversion (see Section 4.2.1) at height z_c.

In unstable, fair-weather, daytime conditions and with moderately smooth surfaces, such as short grassland, $|L|$ is typically within the range 5 to 50 m. Hence, the properties of the lowest layers of the atmosphere are important to the design of telescope installations, particularly at solar observatories, which operate in the daytime. An example of the variation of

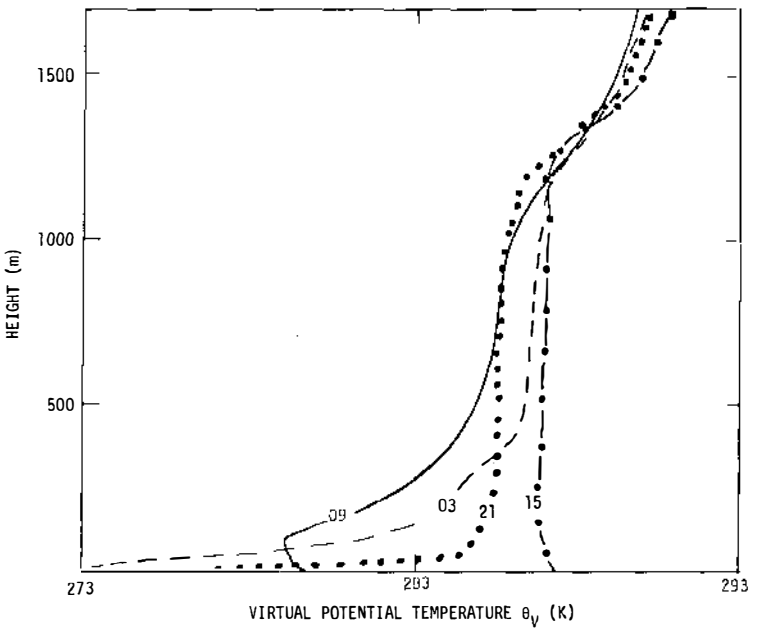

Figure 1 Typical 24-h evolution of stratification in the planetary boundary layer over flatland. The development of a well-mixed layer from $z_c = 100$ m depth at 0900 h (local time) to 1200 m at 1500 h results from surface heating and convection. Cooling after sunset leads to formation of the surface inversion layer seen at 2100 and 0300 h. Above the inversion (~ 1200 m), the profiles respond only weakly to the diurnal cycle. This example is from an actual observation, but the temperatures, heights, and profiles encountered in nature vary widely.

C_N over a 24-h period is given by Clifford (48) from C_T^2 data of Lawrence et al. (162).

Relations of the type discussed here refer to the long-term average values of C_T^2; it is in the nature of turbulence that on a short-term basis large fluctuations from this average occur intermittently. Experimental confirmation rests on data obtained by Coulman (62, 63), Kallistratova & Timanovski (146), and Neff (201); details of the calculation of C_T^2 may be found in Webb (265), Wyngaard & Coté (271), and Wyngaard et al. (273).

The turbulent fluctuations of temperature in convective updrafts greatly exceed those in the associated downward flow (247), and the fluctuation amplitudes usually decrease with height above the ground. Consequently, there is an advantage in locating a solar telescope objective as high as is economically possible above the surrounding terrain, as shown by Kiepenheuer (147) and Coulman (62, 64, 67).

The atmospheric boundary layer above water often exhibits smaller temperature fluctuations than those found over land at similar heights because the temperature contrast between surface and air is frequently smaller (see 51, 89, 190, 225, 263, 264, 279). It has been suggested that observatories could be advantageously sited on an island or a shoreline [for example, by Kiepenheuer (147) and Hansen & Hansen (123)], but very close proximity to the shore is required because the lower layers of an onshore airstream quickly adapt to the land surface conditions (22).

4.1.5 NEUTRAL AND STABLE STRATIFICATION Stable conditions are common at night (44) and in the early morning, as indicated in Figure 1, and research has largely been directed toward the prediction of the bulk properties of stable layers, particularly the evolution of layer depth (see, for example, 43, 204, 276). However, Kaimal (143) showed that C_T^2 could be calculated from his observational data by a relation

$$C_T^2 = 12(R_i)^{2/3}\sigma_T^2 z^{-2/3}, \qquad 4.14$$

which is valid in the lowest one tenth of the stable layer. Here, σ_T^2 is the measured temperature variance.

Brost & Wyngaard (32) consider that the effects of surface energy budget, terrain slope, and radiation balance seldom act to produce steady-state conditions in times short compared with one night, but the observations of Caughey et al. (45) give at least tentative support to Equation 4.14. The same results support the conclusion (273) that above the lowest one tenth of the stable layer, the decrease of C_T^2 with height is less rapid than a $z^{-2/3}$ relation.

Comparatively few direct measurements of C_T^2 (or C_N^2) have been made under stable conditions, but those of Tsvang (252) and Kallistratova &

Timanovski (146) can be said to be not inconsistent with present theoretical treatments. However, recent measurements by Kunkel & Walters (156) suggest intermittent turbulence even at high positive values of R_i.

4.2 *The Free Atmosphere*

Occasions of excellent seeing provide astronomers with valuable, if rather rare, circumstances in which to make important observations. To take advantage of such occasions, they need more detailed predictive information than just a measure of the range of variability of the C_N^2 profile; progress in the prediction of seeing conditions requires an understanding of the processes that relate small-scale refractive inhomogeneity to large-scale atmospheric weather phenomena.

4.2.1 THE DIURNAL CYCLE IN THE PLANETARY BOUNDARY LAYER Solar heating of the surface of the Earth during daytime and subsequent cooling at night lead to a marked cycle of events in the planetary boundary layer (Figure 1). During daytime, in fair weather and over flatland, this layer increases in depth after sunrise to reach a typical maximum of about 1.5 km in midlatitudes by early afternoon; the bulk of it is well mixed by convection, and we have $\partial\theta_v/\partial z \to 0$. However, it is important to realize that this refers to the *area-averaged* θ_v, for the structure of convection is characterized by upward- and downward-moving elements of appreciably different temperatures (68, 179). In disturbed weather, and in the tropics particularly, cumulus cloud growth leads to a planetary boundary layer of 3 km or more in depth. After sunset, convective mixing becomes greatly reduced, and a nocturnal inversion develops near the surface (Figure 1) in response to radiative transfer and comparatively weak turbulence (3).

A general indication of the expected behavior of C_N^2 and C_T^2 in the boundary layer may be obtained from profiles of potential temperature variance $\langle\theta'^2\rangle$, which are extensively treated in the meteorological literature; however, a paper by Wyngaard & Le Mone (272) concerns the behavior of C_N^2 specifically.

In the unstable, daytime planetary boundary layer, significant scales for normalization of this variance are (*a*) the depth of convection z_c (Figure 1) and (*b*) a scale temperature θ_*, defined as

$$\theta_* = \frac{H_0}{\rho c_p w_*}. \qquad 4.15$$

The convective scale velocity is defined as

$$w_* = \left[\frac{gH_0 z_c}{\theta\rho c_p}\right]^{1/3}, \qquad 4.16$$

where H_0 is the surface heat flux.

The behavior of the normalized temperature variance $\langle\theta'^2\rangle/\theta_*^2$ is shown schematically in Figure 2 as a function of normalized height z/z_c. In the range $0 < z/z_c < 0.8$, the relation (273)

$$\frac{\langle\theta'^2\rangle}{\theta_*^2} = 1.8\left(\frac{z}{z_c}\right)^{-2/3} \qquad 4.17$$

holds, but a different normalization scheme is necessary to represent the increased variance that is found between $z/z_c \approx 0.9$ and 1.1 close to the capping inversion layer (2, 145, 219, 253, 254). There is also evidence of larger-scale (e.g. hundreds of meters horizontally) intermittency (68), which is consistent with the observations of brief periods of good daytime seeing referred to by Bray & Loughhead (29) and Coulman & Hall (71).

Under stable, night conditions a comprehensive similarity theory has not yet been developed (270). However, numerical integration of the equations for transfer of sensible heat, humidity, momentum and radiation by André

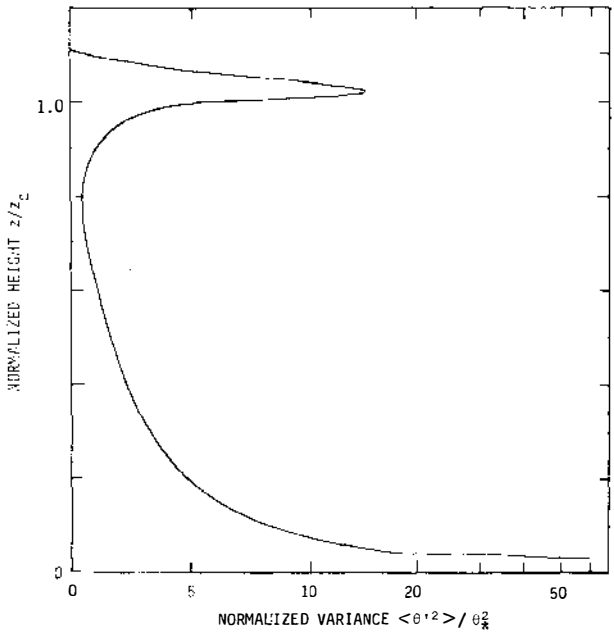

Figure 2 In the daytime surface boundary layer and in the layer well-mixed by convection (total depth z_c), the variance of temperature, and hence of refractive index, decreases rapidly with height until the vicinity of the capping inversion is reached ($z/z_c \approx 0.9$). Mixing across the inversion causes a secondary maximum in variance. Note that the abscissa scale is logarithmic for values greater than 10.

et al. (3), using the data of Clarke et al. (47), shows how layers having enhanced temperature variance can be formed in the nocturnal planetary boundary layer (Figure 3). Enhanced levels of temperature structure were discovered in the boundary layer and elsewhere by Coulman (66) and Bufton (39) using special radiosondes.

4.2.2 TEMPERATURE STRUCTURE ABOVE THE PLANETARY BOUNDARY LAYER Information on the small-scale temperature structure, and hence the refractive index structure above the boundary layer, is available from balloon-borne experiments by Coulman (66), Bufton (39), and Barletti et al. (14), and from scintillation measurements by Azouit & Vernin (8) and Vernin & Roddier (256). These authors, and more specifically Bufton (40), have attempted to correlate the occurrence of layers of enhanced C_T^2 values with other meteorological measurements.

Observations with radar have confirmed the existence of thin layers having high values of wind shear and stable temperature gradients (see, for example, 35, 36, 152, 160, 161); detailed analysis of radiosonde data by Downey et al. (90) has given similar results.

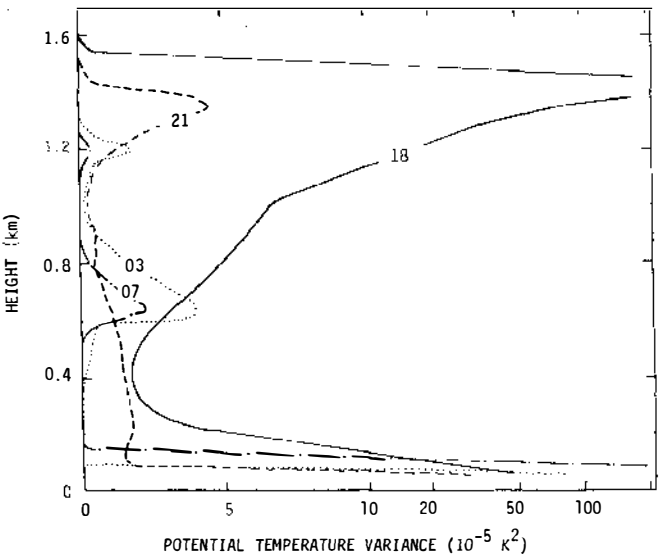

Figure 3 Numerical models by André et al (3) of the stably stratified planetary boundary layer demonstrate that layers of enhanced temperature variance typically form as radiative cooling progresses and turbulence weakens during calm nights. Compare with layers exhibiting large C_N^2 values in Figure 4.

Although the agreement between such independent investigations lends confidence to the profiles of C_T^2 now widely in use for calculating typical seeing quality, it does little to improve the forecasting of seeing at particular places or times. However, it now appears from the above-mentioned numerical work of André et al. (3) and André & Mahrt (4) that the interaction of moderate turbulence and strong nocturnal radiative cooling is important in the formation of these layers. Radiative transfer is increased by increased water vapor content of the air, and so moisture may play an important, if indirect, role in determining seeing quality; the seeing on any night may be influenced by cumulus cloud activity of the preceding days. Furthermore, wind shear and wind direction are dependent upon the prevailing weather pattern, and so it would appear that the conclusion of Barletti et al. (14) that "the optical quality of the impinging air mass is the same" over wide geographical limits above 4000 m altitude should not be too readily accepted as being generally true.

4.2.3 THE EFFECTS OF TERRAIN Quite small undulations affect the dynamics of the boundary layer, while mountains produce lee waves of major proportions. A moist atmosphere is especially sensitive to vertical displacements because condensation, cloud formation, and precipitation may be induced, with possible results like those mentioned in Section 4.2.2. Airflow over mountains has been reviewed by several authors (see 52, 216, 235).

Recent work by Kaimal et al. (144) has shown that gently undulating terrain has only minor effects on the spectral characteristics of turbulence in the convective boundary layer, so we may conclude that the treatment of seeing, as outlined in Section 3, is appropriate for such conditions.

Calculation of the flow field over hilly terrain has been achieved, for example, by Jackson & Hunt (139) and Mason & Sykes (180). The unperturbed flow is represented by Equation 4.13 in neutral conditions, and the shape of the hill by an equation of the form

$$z_h = h \cdot f(x/L_h, y/L_h), \qquad 4.18$$

where h is the height of a hill with a half-width L_h. The perturbed flow field is then calculated as

$$U = U_0(z - z_h) + \varepsilon_1 u_* V\left(\frac{x}{L_h}, \frac{y}{L_h}, \frac{z - z_h}{l_h}\right), \qquad 4.19$$

with an analogous equation for the V-field in the y-direction. The flow is modeled as comprising an outer region that provides the pressure field to drive an inner region, or perturbed boundary layer, of depth l_h; ε_1 is written for a function of l_h, L_h, and z_0.

This approach may be applicable to studies of terrain-produced

atmospheric effects on seeing in the immediate vicinity of a telescope in stable conditions with light wind, particularly at night.

5. QUANTITATIVE TREATMENT OF "SEEING" AND OBSERVATORY SITE SELECTION

The reputation of a given telescope at a given site is too often a matter of opinion. Although it can be argued that objective assessment would be facilitated if astronomers regularly made and recorded quantitative measurements of image quality, it must be remembered that any appreciable sacrifice of astronomical observing time is quite unacceptable. Hence, only methods for making seeing measurements that do not reduce astronomers' telescope time are suitable for continuous monitoring of conditions.

Although direct optical measurements of image quality are usually very convincing, indirect methods yielding data from which seeing quality may be calculated are often less intrusive into telescope usage; furthermore, they are more suitable for the analysis of the contributions to image quality from separate parts of the propagation path.

5.1 *Calculation of System Performance From Microthermal Data*

The MTF of most astronomical instruments is almost that of a diffraction-limited system, and image degradation results from atmospheric effects. The MTF of the system telescope-plus-atmosphere can be calculated from Equations 3.18 or 3.19, provided that the wave structure function $D_W(r)$ can be obtained from Equation 3.13. For light from a celestial source, this equation should be written as

$$D_W(r) = 2.91(2\pi/\lambda)^2 r^{5/3} \sec \omega \int_{z_T}^{z_m} C_N^2(z)\, dz, \qquad 5.1$$

where ω is the angle between zenith and the viewing direction, z_T the telescope height, and z_m the height at which $C_N^2 \to 0$.

The microthermal approach uses C_T^2 values in order to calculate C_N^2 from Equation 4.7. In some circumstances, C_T^2 has been calculated from other meteorological data (e.g. 57, 58) or as outlined in Section 4.1.4; more often, direct measurements have been made with rapid-response resistance thermometers (see, for example, 12, 14, 40, 62, 63, 66, 67, 155, 252). Fast-response thermistors are now used in this kind of work (70).

Hufnagel & Stanley (137) compiled a "typical" atmospheric profile of C_N^2 from published information then available, and simple analytical representations have also been used (see, for example, 220, 277). Observations by

Protheroe & Chen (215) and Ochs & Lawrence (206) suggested that a smooth profile was unrealistic, and Coulman (66), Bufton (39), and Barletti et al. (14, 15) have shown that greatly enhanced values of C_N^2 occur in thin layers throughout the troposphere. A randomly fluctuating model was proposed (136) to synthetically produce a variation with height that exhibits fine structure. Some of these C_N^2 profiles are compared in Figure 4.

Microthermal data are especially useful when applied to the systems design of telescope installations. With a given C_N^2 profile, the parameters that are under the designer's control can be separately investigated for their significance to system performance (64). For example, the height above ground of a telescope objective was examined by Coulman (62), with results illustrated in Figure 5, and the contributions to image degradation may be studied in the immediate vicinity of a telescope (67). A typical layout of

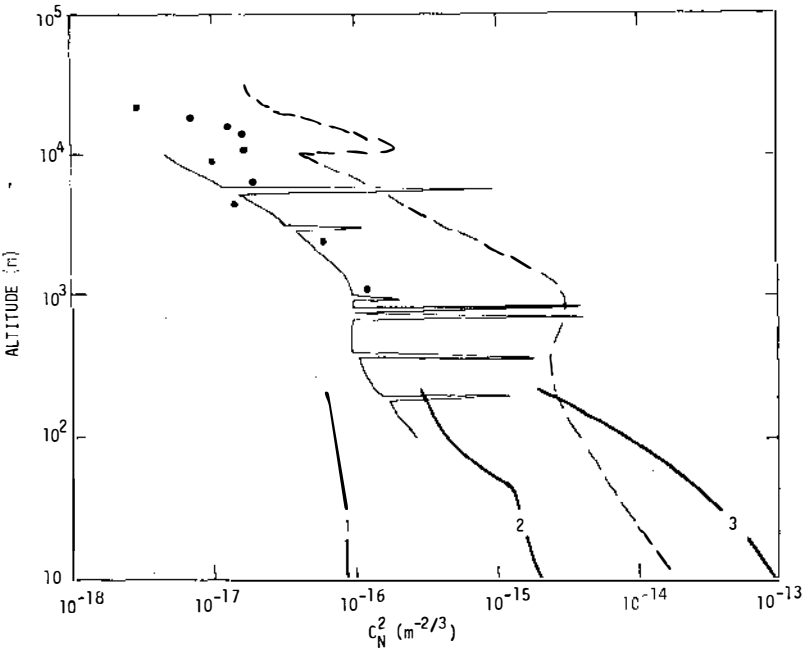

Figure 4 The C_N^2 profile by Hufnagel & Stanley (137) is denoted by a broken line. Observations by Coulman (66) established the occurrence of thin layers of enhanced C_N^2 values; a typical early-morning profile is the thin line. Filled circles are mean values of observations by Bartletti et al. (15), who also found fine structure. Below about 200 m, the profile is diurnally very variable; thick-line 1 is characteristic of good seeing conditions at night, 2 of conditions just before sunset, and 3 of the midday period (62).

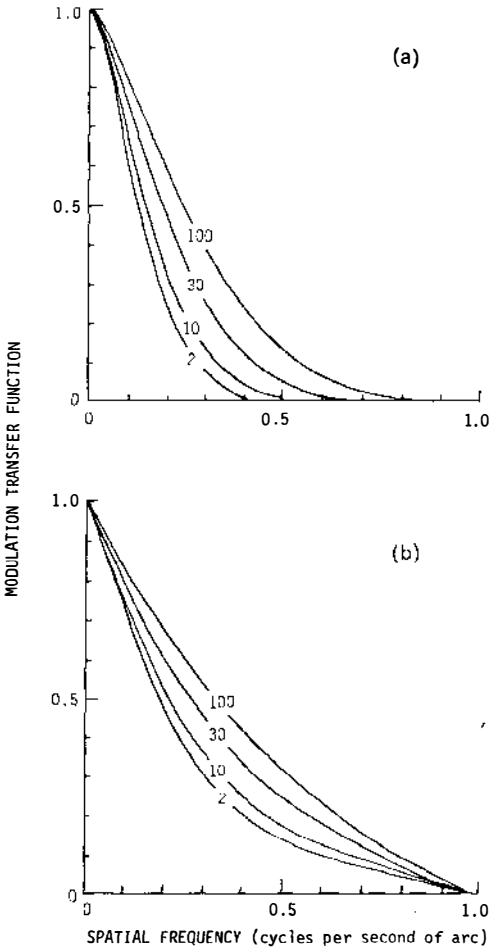

Figure 5 (*a*) The long-exposure MTF of a system comprising atmosphere plus an 11-cm-aperture telescope is shown for four values of height above ground of the telescope objective, indicated in meters. (*b*) The corresponding short-exposure MTF. In both, the C_N^2 profile is typical of midday conditions (62), and the improvements that result from raising the telescope and shortening the exposure time are evident advantages for solar astronomers.

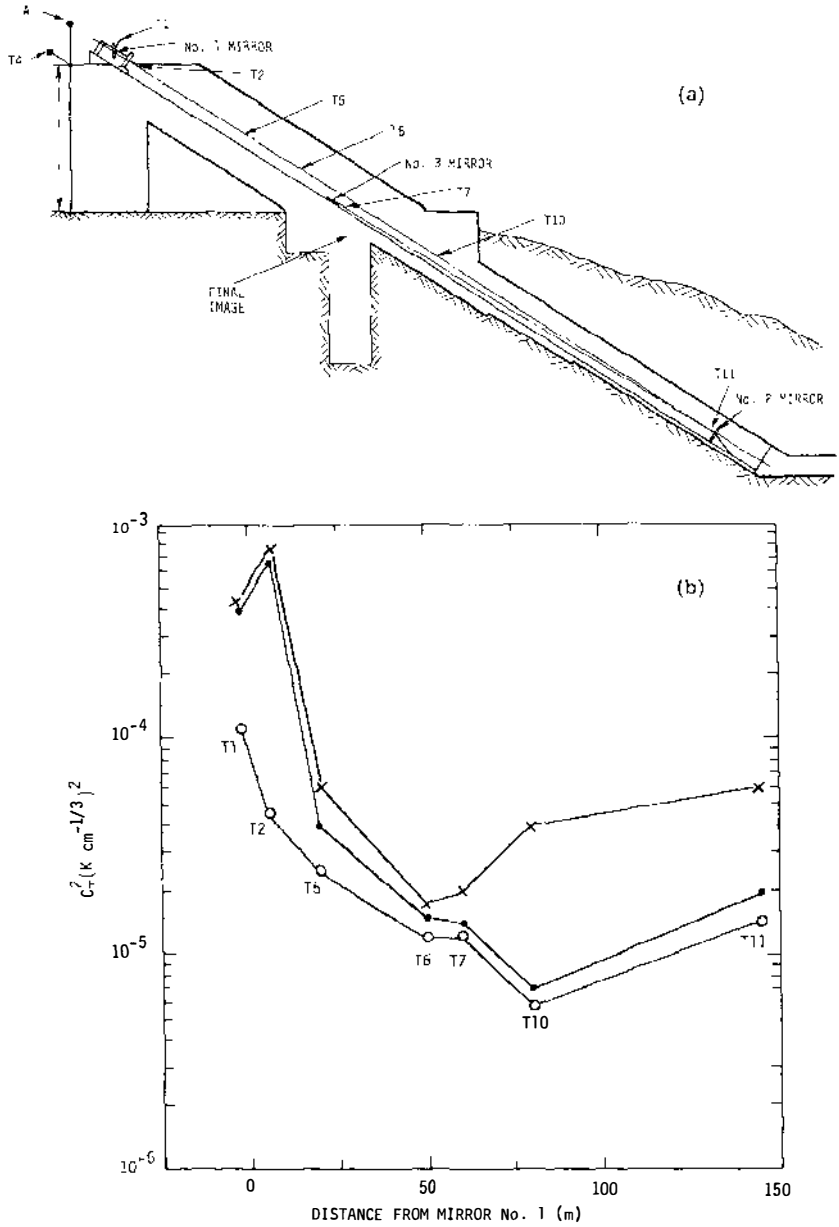

Figure 6 (*a*) A layout of microthermal sensors (T1–T11) in the optical path of the McMath Telescope (1.5-m reflector) at Kitt Peak Observatory. Anemometer is denoted by A. (*b*) Profiles of C_T^2 under several different sets of conditions in the telescope are shown. The effect on the image quality of alterations to conditions may be assessed, and the regions contributing most to the internal seeing identified (see 67).

microthermal sensors and an example of resulting C_T^2 measurements are shown in Figure 6. Similar studies of seeing in and around the dome of a large stellar telescope have been initiated recently by Gillingham (110) and Coulman (70).

An alternative to dispersing microthermal sensors at discrete points along the propagation path was proposed by Hall (116), who used long, thin resistance wires stretched approximately along the optical path.

Other measures of seeing quality calculable from a C_N^2 profile are the Strehl definition of Equation 3.20, and the Fried parameter r_0 of Equations 3.22 and 3.23. Fried (101) chose to write Equation 3.18 in the form

$$\langle M(f)\rangle_{t'\to\infty} = A(f)\exp\{-[3.44(\lambda Ff/r_0)^{5/3}]\}. \qquad 5.2$$

From Equation 5.1 it is apparent that

$$r_0 \propto \left[\int_{z_T}^{z_m} C_N^2(z)\,dz\right]^{-3/5}. \qquad 5.3$$

The parameter r_0 is thus a measure of atmospheric seeing quality, and it has been calculated in connection with site surveys (16).

5.2 *Optical Methods for the Measurement of Seeing*

The quality of astronomical images is generally dependent on the phase fluctuations introduced by the atmosphere, and the amplitude fluctuations across the wave front are usually weak. However, the integrated intensity across the wave front entering a telescope varies in time and causes scintillation of stellar images. There has been a tendency in the literature to separate work on image quality from that on scintillation, and it is convenient, if arbitrary, to review optical image measurements in categories related to the experimental methods used.

5.2.1 SCINTILLATION MEASUREMENTS The logarithmic-amplitude fluctuations χ of a light beam are given by Equation 3.5, and it can be shown (243) that

$$\sigma_I^2 = 4\sigma_\chi^2 = A_1\lambda^{-7/6}(\sec\omega)^{11/6}\int_{z_T}^{z_m} z^{5/6}C_N^2(z)\,dz, \qquad 5.4$$

where σ_I^2 is the "scintillation index" or variance of the relative intensity fluctuations, σ_χ^2 that of the log-amplitude, and $A_1 \approx 19$ a constant.

Thus, for monochromatic light and given zenith angle, σ_I^2 depends only on the C_N^2 profile weighted by a factor $z^{5/6}$, which emphasizes the effect of high-altitude inhomogeneities. Observations (243) using a small-aperture instrument (2 cm) verified Equation 5.4.

Scintillation index formerly was not widely favored as a measure of

observatory site quality; in fact, Stock (236) mentioned seven factors that he considered in his extensive site survey work, and the only one he felt "need not be taken into account" was scintillation.

To a large extent, this view reflects the lack of fundamental understanding of the causes of seeing at that time; more recently, methods have been developed to calculate the C_N^2 profile from higher-order statistics of scintillation. Tatarski (243) has shown that the spatial covariance of amplitude $B_{\mathscr{A}}(r)$ is given by

$$B_{\mathscr{A}}(r) = 4\pi^2 k^2 \int_{z_T}^{z_m} C_N^2(z)\, dz \int_0^{\kappa_m} J_0(\kappa r)\kappa^{-11/3} \sin^2\left[\frac{\kappa^2(z_m - z)}{2(2\pi/\lambda)}\right]\kappa\, d\kappa, \quad 5.5$$

where κ_m is the maximum value of κ. Ochs et al. (207) showed that the first integral in Equation 5.5 can be inverted if measurements of spatially filtered scintillation across a telescope aperture are made, and thus the vertical profile of C_N^2 is calculable, albeit with height resolution poor by comparison with that of microthermal soundings. Vernin & Roddier (256) achieved similar results, and Rocca et al. (222) suggested the use of double stars as test objects to improve height resolution. This suggestion was confirmed by Azouit & Vernin (8).

The regular monitoring of C_N^2 profiles by means of scintillation measurements can now be carried out at observatories and potential observatory sites with automatic recording equipment (169).

5.2.2 INTERFEROMETRIC MEASUREMENTS Although interferometers have been used for measuring the image quality produced by astronomical optical components for a very long time, their use for seeing measurements is of fairly recent origin. Danjon (82) used a Mach interferometer to assess stellar images, and a shearing instrument (18) was used by Coulman & Norton (72) to examine the internal seeing in a refracting telescope.

The first interferometric measurements of the phase structure function $D_S(r)$ were made by Coulman (59) with a birefringent shearing interferometer. If the wave front converging to a focus is perfectly spherical, the fringes in the overlap sheared region of images will not depend upon the shear; for a deformed wave front the change in order of interference Δm at a distance x from the origin along the axis of shear is

$$\Delta m = \frac{1}{2\pi}[S(x) - S(x-a)], \quad 5.6$$

where a is the linear shear. The structure function is then calculable as

$$D_S(a) = \langle [S(x) - S(x-a)]^2 \rangle. \quad 5.7$$

A multichannel shearing interferometer capable of simultaneous measurements at three values of the shear a has been described (63) for verification of the two-thirds law in homogeneous turbulence.

The MTF may be measured interferometrically by directly obtaining the exponential term in Equation 3.18. This term, the mutual coherence function, was measured for stellar sources with an interferometer devised by Roddier & Roddier (224) and later by Breckinridge (30, 31), Dainty & Scaddan (80), and Brown & Scaddan (34). The work of Dainty & Scaddan amounted to an assessment of observatory site quality over a short period (about 10 days) and therefore represents an important step in quantitative site testing.

The technique of speckle interferometry is dealt with in Section 6.

5.2.3 OPTICAL METHODS FOR SITE SELECTION AND IMAGE MONITORING It was evident by about 1960 that photoelectric and photographic methods were the norm for observatory site-selection expeditions (74, 236), although visual methods have been occasionally utilized more recently by, for example, Kiepenheuer (147) and Coulman (56). Babcock (10) used a fine graticule in the focal plane of a telescope to analyze photoelectrically the image tremor, and Harlan & Walker (127) employed star-trail photography, originated by Couder (55), using the width of the photographic image of a star as a measure of long exposure image blur. Stock & Keller (237) developed a double-beam telescope, in which image motion is observed as relative motion of two images formed by the separate beams, thus overcoming the problem of telescope vibration.

The Foucault test, in which the image is partly occulted by a knife edge, has been used as a means of estimating seeing quality (227), and occultation is also used in the photoelectric Polaris Image-Motion Analyzer (PIMA; see 173, 183).

The use of the Hartmann test to measure seeing visually is attributable to Rösch (226), and it has been used with photographic recording by Miller & Kellen (188) and with a digitized video-receiver by Gillingham (109). The latter made novel tests of the effect of a large dome on local seeing by simultaneous monitoring of the Hartmann images given by a 3.9-m telescope within the dome and those formed by a small telescope mounted outside the dome.

A stellar image monitor, which utilizes a rotating sector-disk and photoelectric detector, was developed by Ramsay & Kobler (218) to give outputs proportional to the real and imaginary parts of the OTF; surprisingly it has been used in only one site survey (208), although Coulman (57, 58) used it for fundamental studies of optical propagation. A simple solar seeing monitor has been described (29) for triggering

photographic exposures at moments of good seeing, and a more versatile instrument, useful for analysis of image motion and blurring, was made by Brandt (27, 28) and developed by Borgnino et al. (24).

Traditional site-testing campaigns have utilized some of the simpler instruments and methods just described. An early example is the campaign that resulted in the choice of Kitt Peak, Arizona (184); accounts of the techniques used and results obtained have been given (173, 183, 236). Dommanget (88) gave an account of site testing in South Africa, Stock (236) briefly reported on the choice of Cerro Tololo in Chile, and Hogg (133) described visual seeing tests that led to selection of the Siding Spring Mountain site in Australia.

The selection of Mauna Kea as the site for the University of Hawaii's large telescope resulted from a traditional survey conducted with visual instruments, star-trail photography with double-beam telescopes, and Babcock-type seeing monitors. The campaigns are described by Jefferies & Zirker (142) and Jefferies & Sinton (141). Meteorological investigations, including some microthermal measurements, were made by McKnight & Jefferies (177) and Morrison et al. (195).

Walker (257) carried out tests at numerous sites in California and later in Arizona, Baja California, Chile, and Australia (258); that traditional methods are still in use is evidenced by the work of McInnes & Walker (176) and McInnes (175).

A more quantitative approach to site-testing is now possible as a result of improved understanding of the physical mechanism of atmospheric degradation of images. Tatarski (244) showed that the variance of angle-of-arrival of rays at a star image (σ_α^2) can be written as

$$\sigma_\alpha^2 = \left(\frac{\lambda}{2\pi}\right)^2 \cdot \frac{D_S(r_L)}{r_L^2}, \qquad 5.8$$

and from Equation 5.1 we have that the mean-square image movement is therefore

$$\sigma_\alpha^2 = \text{constant} \times r_L^{-1/3} \sec \omega \int_{z_T}^{z_m} C_N^2(z)\, dz. \qquad 5.9$$

With the constant given by Fried (100), we have

$$\sigma_\alpha^2 = 0.358\left(\frac{\lambda}{r_L}\right)^{1/3}\left(\frac{\lambda}{r_0}\right)^{5/3} \text{rad}^2. \qquad 5.10$$

For large telescopes, σ_α^2 may overestimate image motion because of the neglect of a finite outer scale of turbulence beyond which the two-thirds law does not apply (255).

Image movement (or first-order tilt of the wave front) does not affect the quality of the short-exposure image (61, 101). The MTF for a short exposure is given by Equation 3.19, and hence from Equations 3.21 and 5.2 we obtain the resolution $\mathscr{R}$ corresponding to the short-exposure image blur. It is convenient to define the angular diameter γ of a uniform-intensity blur-disk having the same integrated intensity as the short-exposure image. Equation 5.3 then leads to

$$\gamma = 1.268 \frac{\lambda}{r_0} \qquad 5.11$$

for a telescope aperture large by comparison with the scale of refractive index fluctuations. The interrelationship of σ_α^2 and γ is not simple; Roddier (223) expressed this graphically as a function of r_L/r_0.

The probability of getting an image with wave-front distortion not exceeding some specified value has been calculated by Fried (103); for this value to be, say, 10^{-3} the telescope aperture must be restricted to about $7r_0$. For a high-intensity source, good results are obtained by selecting from many short-exposure images formed by a comparatively small telescope (196).

The evaluation of Mount Hopkins, Arizona, as an observatory site involved the use of traditional methods, MTF measurements, and micro-thermal soundings, as reported by Pearlman et al. (208, 209) on the basis of plans described by Coulman (60).

A comprehensive campaign has been conducted by the Joint Organization for Solar Observations. A 10-year period of activity has been summarized (1), and lists of internal JOSO reports appear in the annual reports (from 1971 onward) by de Jager (85). Visual assessments (178), microthermal soundings by aircraft (148, 149) and radiosondes (13), star-trail photography analyzed by modern methods to yield quantitative resolving-power measurements (194), and photoelectric analysis of solar limb motion by Brandt (27, 28) and Borgnino et al. (24, 25) have all been featured in the JOSO program.

Other surveys during the past decade were conducted by Cuffey (76), Walters et al. (262), Walters (260), and Walters & Kunkel (261) in New Mexico and by Hartley et al. (129) and Smith (234) in the Canary Islands.

6. TECHNIQUES FOR MINIMIZING IMAGE-DEGRADING EFFECTS OF THE ATMOSPHERE

Although this subject is not strictly concerned with the study of seeing per se, it is nevertheless appropriate to review the available methods for

minimizing the undesirable effects of the atmosphere. Other reviews of high-resolution techniques have appeared recently (e.g. 50, 223, 250, 269).

6.1 *Amelioration of Local Seeing Conditions*

The most obvious method for ameliorating seeing conditions is the reduction, where possible, of the magnitude of refractive-index fluctuations in the propagation path. After selecting an observatory site, reductions in image-degrading effects can be achieved by modifications to telescopes or their immediate surroundings. Solar installations are usually susceptible to such improvement because of the large daytime contribution to atmospheric inhomogeneity in the lowest few tens of meters of air (62, 67).

Recognition of this fact led to the construction of solar tower telescopes early in the twentieth century, a period reviewed by Bray & Loughhead (29). Efforts to minimize the seeing effects of domes and enclosures for solar telescopes were made by Rösch (228) and Kiepenheuer (147). Free-standing instruments on level sites were pioneered by Coulman (56), Bray & Loughhead (29), and Loughhead et al. (170), and telescopes with all or part of their internal optical paths in vacuo are described by Dunn (92), Mayfield et al. (182), and Livingston et al. (168). The use of helium-filled telescopes to minimize internal seeing effects while improving the heat transfer from optical components is mentioned by Engvold et al. (97).

Microthermal and optical techniques (Section 5) have led to modifications in the shielding and the ventilation of solar instruments (see 25, 29, 59, 65, 67), while Coulman (64) showed how microthermal measurements could be used in cost-benefit analysis for the design of solar telescope towers.

At stellar observatories, improvement has mainly been concerned with reducing the inside-to-outside temperature difference across the aperture of telescope domes. Measurements specifically aimed at estimating the magnitude of this effect have been made by Murdin & Bingham (199) and Gillingham (109, 110). A widely used remedy has been the installation of refrigeration within the dome and telescope structure—for example, in the Kitt Peak 4-m telescope (132) and in the CFH reflector at Hawaii (232). Gillingham (110) achieved important improvements to the Anglo-Australian Observatory telescope with augmented fan ventilation, and further developments are proposed by Coulman (70). Discussion of the seeing problems associated with domes are touched upon in various papers (19, 75, 98, 106, 153, 187).

6.2 *Image Analysis and Processing*

6.2.1 USE OF THE OPTICAL TRANSFER FUNCTION Arising from the application of Fourier transforms to optics (91) and the development of optical

transfer function theory (Section 3), the possibility of reconstructing, or restoring, a degraded image was canvassed by Elias et al. (96), and Hufnagel (135). Clearly, processing cannot increase the information content of the received image, but given some measure of the degrading effect, such as the atmospheric MTF, the probability of successful visual recognition of certain features of an image can be enhanced.

If we represent the intensity distribution in the image plane by $I(\eta, \zeta)$ for an ideal, nondegraded image and by $I'(\eta, \zeta)$ for the degraded image, then we may relate their Fourier transforms through the MTF of the system (91):

$$\hat{F}\{I'(\eta, \zeta)\} = \hat{F}\{I(\eta, \zeta)\}\hat{F}\{s(\eta, \zeta)\}. \qquad 6.1$$

As in Section 3, the function $s(\eta, \zeta)$ represents the intensity distribution in the image of an incoherent, luminous point object and $\hat{F}$ is the Fourier transform operator. Hence, in principle, if sufficient information is available to calculate the MTF (as discussed in Section 5), the nondegraded image can be reconstructed by solution of Equation 6.1 for $I(\eta, \zeta)$.

This approach was shown to be feasible by Harris (128) in the case of linear image motion in the laboratory. The situation is complicated when applied to seeing-degraded astronomical images by the fact that the spread function is neither (*a*) time-variant (because seeing fluctuates rapidly) nor (*b*) space-invariant (because seeing is usually different along differently oriented propagation directions). The region over which it is invariant is the *isoplanatic region*. Subject to these limitations, it is possible to restore images either by including in the field of view the image of a star from which to calculate the MTF or by prior knowledge of some features of the object's light distribution. The former method is exemplified by Hawkins (131), while Coupinot (73) used the latter; generally such image processing is carried out digitally, as described in detail by Andrews & Hunt (5), and the limitations of the method are reviewed by Goodman & Belsher (112) and Goodman (111). A comparison of analog-optical and digital methods has been made by Lüke (171).

Reconstruction of both short- and long-exposure images has been attempted, for example, by McGlamery (174); the modulation transfer functions relevant to such processing are as given in Equations 3.18 and 3.19, respectively, but the use of a Gaussian form has been often favored for numerical convenience (e.g. 131, 174). Computational aspects were extensively treated at an International Workshop on Image Processing at Trieste in 1979, at which Fellgett (99) discussed the recognition of detail in restored images.

6.2.2 SPECKLE TECHNIQUES Labeyrie (157) suggested a novel way of using the information contained in the short-exposure image, or speckle pattern,

of a point source to obtain resolution approaching that of a diffraction-limited system.

The speckle technique uses the averaged, squared modulus of the Fourier-transformed image intensity; thus, we have

$$\langle|\hat{F}\{I(\eta,\zeta)\}|^2\rangle = \langle|\hat{F}\{O(\eta,\zeta)\}|^2\rangle \cdot \langle|\hat{F}\{s(\eta,\zeta)\}|^2\rangle, \qquad 6.2$$

where O denotes the object intensity distribution, I the image distribution, and angle brackets the ensemble averaging operation over many images. For an unresolved point source, this amounts to measuring the averaged, squared modulation transfer function, i.e. the second factor on the right-hand side of Equation 6.2. Gezari et al. (108) used photographic summation of star images and analog Fourier transformation techniques to obtain the power spectra. Hence, the diameters of stars were deduced. This method has been applied by many workers (e.g. 21).

The term speckle imaging has been coined for a process in which the phase as well as the modulus of the Fourier transform is retained, and the method is thus made applicable to arbitrarily shaped light distributions in objects that do not have simple symmetry (150). Walker (259) has proposed a novel method for the digital processing of speckle images that permits unambiguous retrieval of modulus and phase information; as yet, however, it has been tested only by computer simulation. Huiser (138) split a star image into two by means of a semitransparent mirror followed by the use of different spatial filters (or pupil functions) for each secondary image. Recombination then allows retrieval of the information necessary to reconstruct an object having arbitrary light distribution or symmetry.

Korff (154) considered the requirements of the image-averaging process, Fried (104) discussed the isoplanatism conditions necessary, and Dainty & Greenaway (79), among others, provided a signal-to-noise analysis for speckle interferometry. Photoelectric image detection probably leads to better signal-to-noise ratios than does photography (221), and it also permits the technique to be extended to the infrared (164).

6.2.3 INTERFEROMETERS AND TELESCOPE ARRAYS These instruments are able to minimize the effects of seeing by using measurements of certain functions of the image intensity distribution; they may therefore be considered as examples of image analysis and processing.

Intensity interferometry, pioneered by Hanbury Brown & Twiss (122) and Hanbury Brown (118), uses two large mirrors, separated by distance d, to collect starlight, which is detected photoelectrically (B_1, B_2 in Figure 7*a*) and fed to an electronic correlator X. A simplified analysis considers one Fourier component of the light from one part of a star at frequency ω_1, and another component ω_2 from some other part of the star; the signal $i(B_1)$ at

detector B_1 is given by

$$i(B_1) \propto [A_1 \sin(\omega_1 t + \phi_1) + A_2 \sin(\omega_2 t + \phi_2)]^2, \quad 6.3$$

and at B_2 by

$$i(B_2) \propto [A_1 \sin\{\omega_1(t + d_1/c) + \phi_1\} + A_2 \sin\{\omega_2(t + d_2/c) + \phi_2\}]^2. \quad 6.4$$

Here A_1, A_2 are measures of amplitude, ϕ_1, ϕ_2 arbitrary phases, t time, c the

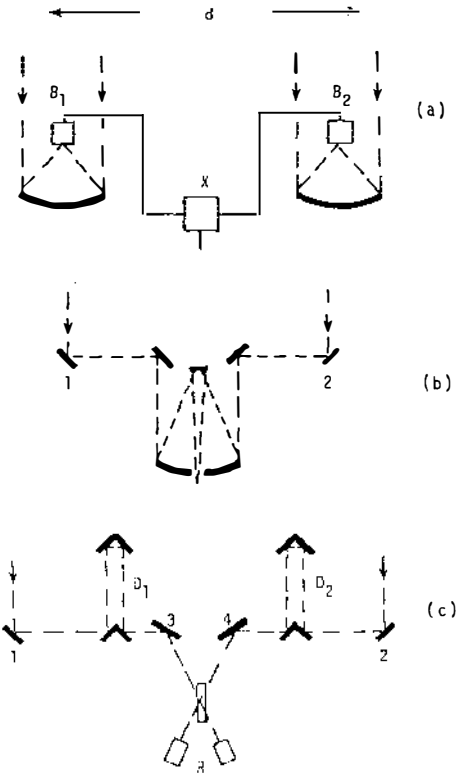

Figure 7 (*a*) Intensity interferometry is carried out with two optical receivers separated by a variable distance *d*. The signals from photoelectric sensors B_1, B_2 are correlated at X. Tolerances on equality of path length in the two beams are relaxed by a factor of about 10^6 when compared with amplitude interferometers. (*b*) The Michelson interferometer uses two separated receivers (1 and 2). The diameter of these must be smaller than r_0, which characterizes the quality of seeing. Resolution for stellar images approaches that of a telescope of diameter equal to the separation of 1 and 2. (*c*) A modern version of the Michelson interferometer, which employs dynamic optical components 3, 4, D_1, and D_2 to compensate for the effects of atmospheric seeing, is under development by Davis (84) and others.

velocity of light, and d_1, d_2 the phase lags between the detected signals expressed in terms of mirror separation.

Expansion of Equations 6.3 and 6.4 leads to terms in $2\omega_1, 2\omega_2, (\omega_1+\omega_2)$, and $(\omega_1-\omega_2)$. The signals at the lowest frequency $(\omega_1-\omega_2)$ are correlated, and the correlation function $B(d)$ is (with $\omega = \omega_1 \approx \omega_2$)

$$B(d) \propto A_1^2 A_2^2 \cos[(\omega/c)(d_1-d_2)]$$
$$\propto A_1^2 A_2^2 \cos 2\pi d(\theta/\lambda), \qquad 6.5$$

where θ is the angular separation between points 1 and 2 on the star. Hence, stellar angular diameters can be measured using the correlation between signals at the relatively low frequency $(\omega_1-\omega_2) \approx 10^8$ Hz compared with 10^{14} Hz $\approx \omega_1 \approx \omega_2$ for visible light. The wavelength corresponding to $(\omega_1-\omega_2)$ is about 10^6 as large as that for ω, and the atmosphere cannot introduce anything like 10^6 wavelengths of path difference between the beams to B_1 and B_2. Similarly, the tolerances on instrument stability are fairly large. Proposals for further work are reviewed by Hanbury Brown (120).

A comparison between intensity interferometry and the classical [Michelson & Pease (186)] interferometer has been made by Hanbury Brown (119). The latter technique is, of course, subject to the effects of atmospheric seeing, and mirrors 1 and 2 in Figure 7*b* have to be "small"; specifically, their diameters should be less than the value r_0 (Section 5).

A modern, servo-compensated version of the Michelson interferometer (Figure 7*c*) was reviewed by Hanbury Brown (119). The coelostats 1 and 2 are guided to keep the star on axis, and rapid tilts of the wave front are corrected by dynamic optical components 3 and 4. Path-length fluctuations are compensated for by dynamic optical systems D_1, D_2 before the summation of the two beams is presented to one of the receivers at R and the difference to the other. Progress in constructing such instruments is described by Davis (84), Tango (242), Hardy & Wallner (124), and Hanbury Brown (121). Other examples of amplitude interferometers are found in Currie (77), Currie et al. (78), and Liewer (165).

Two-aperture interferometry may be considered to be a special case of a telescope array. Labeyrie (158) described an early example of a two-telescope array designed for coherent image analysis and made proposals for an extension to utilize large telescopes (i.e. diameter exceeding r_0) and to employ an array of more than two elements. Dynamic optics are implicitly assumed; designs and proposals have been outlined (114, 159) and problems specific to the infrared considered (7, 54).

Incoherent imagery by arrays of telescopes is a method for obtaining the photometric advantages of a telescope larger than can be made at present as

a single unit. Instruments of this kind are described in Burbidge & Hewitt (41) and by Disney (87) and Strittmatter (238), who have emphasized the need for dynamic optical systems to overcome mechanical instability. Hall (117), however, mentioned a requirement for phase control to permit speckle interferometry, clearly with a view toward attaining resolution not appreciably degraded by seeing.

6.3 *Dynamic Optical Components*

There appears to be no unanimity about the terminology for deformable optical components used in a servo system for compensating optical path fluctuations: The terms dynamic, active, live, and adaptive optics are all commonly used. Recent developments of this technique owe much to the theoretical work by Dyson (93, 94), who provided a basis for systems design of dynamic optical correctors at about the time when experimental work was actively commencing (see, for example, 125, 189, 197, 211). Babcock (9) proposed a method of compensating seeing with the inadequate technology available in 1953.

The essential elements of a dynamic image-correcting system are (*a*) a means of measuring wave-front distortion, (*b*) a processor with servo system, and (*c*) dynamic optical components. The processor outputs signals at time t_2 that are functions of the wave-front distortion sensed at a previous time t_1, and the servo system attempts to eliminate atmospherically caused noise (seeing). Dyson (93) showed that the act of deforming the dynamic components in order to achieve this noise cancellation introduces correlated effects into the photon noise associated with image detection. The statistics of path-length error are thus composed of an atmospheric component that is reduced by the feedback and a photon noise component that is amplified by it; systems design aims to select an optimum solution.

Wave-front distortion is sensed by (*a*) measurement of photometric fine structure (speckle) in the image of a star, or (*b*) measurement of the wave-front slope at numerous points. Buffington et al. (38) have shown, using method (*a*), that the maximization of a function such as S_2, given by

$$S_2 = \int I'(\eta, \zeta) M(\eta, \zeta)\, d\eta\, d\zeta, \qquad 6.6$$

can improve the resolution of a star image. Here M is the transmittance distribution of a suitable mask in the image plane. Improved images of the stars Arcturus and Sirius have demonstrated the successful application of this method (37).

Hardy et al. (126) have successfully applied method (*b*) by utilizing a scanning shearing interferometer; this measurement is described, in principle, by Equation 5.6.

The dynamic correcting element most favored recently is the deformable mirror driven by piezoelectric transducers. Buffington et al. (38) and Mast & Nelson (181) used a mirror composed of separate elements, while Hardy et al. (126) and Grosso & Yellin (115) favored flexible reflectors. A recent report on this technology is given by Pearson (210).

The nature of atmospheric seeing places limitations on dynamic optics that are similar to those placed on the image-processing methods of Section 6.2. Hence, the temporal and spatial variations of seeing impose stationarity and isoplanatic conditions upon the practical methods employed to correct images (see 100–102, 104, 231).

ACKNOWLEDGMENTS

I am indebted to the late Dr. R. G. Giovanelli, who in 1962 finally persuaded me to take an interest in what I have found to be a fascinating subject.

Literature Cited

1. Alvensleben, A. von 1979. *JOSO Ann. Rep.*, Kiepenheuer Inst. Sonnenphys., Freiburg, Fed. Repub. Ger. 159 pp.
2. André, J. C., Artaz, M. A. 1980. *C. R. Acad. Sci. Paris* 290B: 191–94
3. André, J. C., de Moor, G., Lacarrère, P., Therry, G., du Vachat, R. 1978. *J. Atmos. Sci.* 35: 1861–83
4. André, J. C., Mahrt, L. 1982. *J. Atmos. Sci.* 39: 864–78
5. Andrews, H. C., Hunt, B. R. 1977. *Digital Image Restoration.* Englewood Cliffs, NJ: Prentice-Hall. 238 pp.
6. Antonia, R. A., Chambers, A. J., Friehe, C. A. 1978. *Boundary-Layer Meteorol.* 15: 243–53
7. Assus, P., Choplin, H., Corteggiani, J. P., Cuot, E., Gay, J., et al. 1979. *J. Opt.* 10: 345–50
8. Azouit, M., Vernin, J. 1980. *J. Atmos. Sci.* 37: 1550–57
9. Babcock, H. W. 1953. *Publ. Astron. Soc. Pac.* 65: 229–36
10. Babcock, H. W. 1963. *Publ. Astron. Soc. Pac.* 75: 1–8
11. Barabanenkov, Yu. N., Kravtsov, Yu. A., Rytov, S. M., Tatarski, V. I. 1971. *Sov. Phys.-Usp.* 13: 551–680
12. Barletti, R., Ceppatelli, G., Moroder, E., Paternò, L., Righini, A. 1974. *JOSO Rep. SIT 21*, Florence, Italy
13. Barletti, R., Ceppatelli, G., Paternò, L., Righini, A., Speroni, N. 1975. *JOSO Rep. SIT 27*, Florence, Italy
14. Barletti, R., Ceppatelli, G., Paternò, L., Righini, A., Speroni, N. 1976. *J. Opt. Soc. Am.* 66: 1380–83
15. Barletti, R., Ceppatelli, G., Paternò, L., Righini, A., Speroni, N. 1977. *Astron. Astrophys.* 54: 649–59
16. Barletti, R., Ceppatelli, G., Paternò, L., Righini, A., Speroni, N. 1977. *Appl. Opt.* 16: 2419–21
17. Batchelor, G. K. 1953. *Homogeneous Turbulence.* Cambridge: Cambridge Univ. Press. 197 pp.
18. Bates, W. J. 1947. *Proc. Phys. Soc. London* 59: 940–50
19. Baustian, W. W. 1971. *Proc. ESO/CERN Conf. Large Telesc. Des.*, ed. M. West, pp. 351–57. Geneva: ESO/CERN
20. Bean, B. R., Dutton, E. J. 1966. *Radio Meteorology, NBS Monogr. 92.* Reprinted 1968, New York: Dover. 435 pp.
21. Beddoes, D. R., Dainty, J. C., Morgan, B. L., Scaddan, R. J. 1976. *J. Opt. Soc. Am.* 66: 1247
22. Berry, G. V., Ward, R. C. 1967. *Aerosp. Corp. Los Angeles Rep. No. TR-1001 (2203-25)-6.* 37 pp.
23. Booker, H. G., Ratcliffe, J. A., Shinn, D. H. 1950. *Philos. Trans. R. Soc. London Ser. A* 242: 579–609
24. Borgnino, J., Vernin, J., Aime, C., Ricort, G. 1979. *Sol. Phys.* 64: 403–15
25. Borgnino, J., Azouit, M., Barletti, R., Ceppatelli, G., Paternò, L., et al. 1979. *Astron. Astrophys.* 79: 184–89
26. Born, M., Wolf, E. 1970. *Principles of Optics.* Oxford: Pergamon. 808 pp. 4th ed.

27. Brandt, P. N. 1969. *Sol. Phys.* 7:187–203
28. Brandt, P. N. 1970. *Sol. Phys.* 13:243–46
29. Bray, R. J., Loughhead, R. E. 1964. *Sunspots*. London: Chapman & Hall. 303 pp.
30. Breckinridge, J.B. 1975. *J. Opt. Soc. Am.* 65:755–59
31. Breckinridge, J. B. 1976. *J. Opt. Soc. Am.* 66:143–44
32. Brost, R. A., Wyngaard, J. C. 1978. *J. Atmos. Sci.* 35:1427–40
33. Brown, D. S. 1980. *Proc. Conf. Opt. Telesc. for the 1990s*, pp. 999–1005. Tucson: Kitt Peak Natl. Obs.
34. Brown, D. S., Scaddan, R. J. 1979. *Observatory* 99:125–28
35. Browning, K. A. 1971. *Q. J. R. Meteorol. Soc.* 97:283–99
36. Browning, K. A., James, P. K., Parkes, D. M., Rowley, C., Whyman, A. J. 1978. *Nature* 271:529–31
37. Buffington, A., Crawford, F. S., Muller, R. A., Orth, C. D. 1977. *J. Opt. Soc. Am.* 67:304–5
38. Buffington, A., Crawford, F. S., Muller, R. A., Schwemin, A. J., Smits, R. G. 1977. *J. Opt. Soc. Am.* 67:298–303
39. Bufton, J. L. 1973. *Appl. Opt.* 12:1785–93
40. Bufton, J. L. 1973. *J. Atmos. Sci.* 30:83–87
41. Burbidge, G., Hewitt, A., eds. 1981. *Telescopes for the 1980s*. Palo Alto, Calif: Ann. Rev. 278 pp.
42. Burke, R. B. 1962. Translation of *Opus Major*, Roger Bacon, Vol. 2, Chap. 7. New York: Russell. 387 pp.
43. Businger, J. A., Arya, S. P. S. 1974. *Adv. Geophys.* 18A:73–92
44. Byzova, N. L. 1978. *Sov. Meteorol. Hydrol.* 5:32–36
45. Caughey, S. J., Wyngaard, J. C., Kaimal, J. C. 1979. *J. Atmos. Sci.* 36:1041–52
46. Chernov, L. A. 1958. *Wave Propagation in a Random Medium*. Transl. R. A. Silverman, 1960. New York: Dover. 168 pp.
47. Clarke, R. H., Dyer, A. J., Brook, R. R., Reid, D. G., Troup, A. J. 1971. *Pap. No. 19*, Div. Meteorol. Phys., CSIRO, Melbourne, Aust.
48. Clifford, S. F. 1978. *Top. Appl. Phys.* 25:9–41
49. Clifford, S. F., Ochs, G. R., Lawrence, R. S. 1974. *J. Opt. Soc. Am.* 64:148–54
50. Code, A. D. 1973. *Ann. Rev. Astron. Astrophys.* 11:239–68
51. Cooper, A. W., Crittenden, E. C., Schroeder, A. F. 1974. In *Digest of Topical Meeting on Optical Propagation Through Turbulence*, ed. F. F. Hall, pp. WB4-1–4. Boulder: Univ. Colo.
52. Corby, G. A. 1954. *Q. J. R. Meteorol. Soc.* 80:491–521
53. Corrsin, S. 1951. *J. Appl. Phys.* 22:469–73
54. Corteggiani, J. P., Gay, J., Rabbia, Y. 1979. *J. Opt.* 10:351–53
55. Couder, A. 1936. *C. R. Acad. Sci. Paris* 203:609–11
56. Coulman, C. E. 1963. *Rep. PIR-48*, Div. Phys., CSIRO, Sydney, Aust.
57. Coulman, C. E. 1965. *J. Opt. Soc. Am.* 55:806–12
58. Coulman, C. E. 1966. *J. Opt. Soc. Am.* 56:1232–38
59. Coulman, C. E. 1967. *Proc. Astron. Soc. Aust.* 1:67–68
60. Coulman, C. E. 1968. *A Long-Range Program for Astronomical Observatory Site Evaluation, Rep. for Smithsonian Astrophys. Obs.*, Div. Phys., CSIRO, Sydney, Aust.
61. Coulman, C. E. 1968. *J. Opt. Soc. Am.* 58:1668–69
62. Coulman, C. E. 1969. *Sol. Phys.* 7:122–43
63. Coulman, C. E. 1969. *Optical "seeing" in the atmosphere above level terrain*. PhD thesis. Univ. London, Engl. 195 pp.
64. Coulman, C. E. 1970. In *Optical Instruments and Techniques*, ed. J. H. Dickson, pp. 528–37. Newcastle, Engl: Oriel
65. Coulman, C. E. 1972. *A Study of Microthermal Conditions in and Around the McMath Solar Telescope, Kitt Peak Natl. Obs. Consult. Rep.* 30 pp.
66. Coulman, C. E. 1973. *Boundary-Layer Meteorol.* 4:169–77
67. Coulman, C. E. 1974. *Sol. Phys.* 34:491–506
68. Coulman, C. E. 1978. *Boundary-Layer Meteorol.* 14:493–513
69. Coulman, C. E. 1980. *Boundary-Layer Meteorol.* 19:403–20
70. Coulman, C. E. 1982. In *Report of AAT Dome Seeing Review Committee to Anglo-Australian Telescope Board*. Epping, NSW: Anglo-Aust. Obs.
71. Coulman, C. E., Hall, D. N. B. 1967. *Appl. Opt.* 6:497–503
72. Coulman, C. E., Norton, D. G. 1966. *Observatory* 86:210–11
73. Coupinot, G. 1973. *Icarus* 19:212–23
74. Courtès, G. 1963. *Proc. IAU Symp. No. 19, Site Testing*, pp. 155–71
75. Crawford, D. L. 1971. *Proc. ESO/CERN Conf. Large Telesc. Des.*, ed. M. West, pp. 23–36. Geneva: ESO/CERN
76. Cuffey, J. 1978. *Magdalena Peak Obs.*

Site Rep. No. 3, Univ. N.Mex., Albuquerque
77. Currie, D. G. 1967. In *Woods Hole Summer Study*, Vol. 2. Washington, DC: Natl. Acad. Sci.
78. Currie, D. G., Knapp, S. L., Liewer, K. M. 1974. *Ap. J.* 187: 131–34
79. Dainty, J. C., Greenaway, A. H. 1979. *Proc. IAU Colloq. No. 50, High Angular Resolution Stellar Interferometry*, pp. 23-1–18
80. Dainty, J. C., Scaddan, R. J. 1975. *MNRAS* 170: 519–32
81. Danjon, A. 1926. *C. R. Acad. Sci. Paris* 183: 1032–34
82. Danjon, A. 1955. *Vistas Astron.* 1: 377–85
83. Dashen, R. 1979. *J. Math. Phys. (NY)* 20: 894–920
84. Davis, J. 1979. *Proc. IAU Colloq. No. 50, High Angular Resolution Stellar Interferometry*, pp. 14-1–12
85. de Jager, C. 1971. *JOSO Ann. Rep. 1970*, Fraunhofer Inst., Freiburg-im-Br., Fed. Repub. Ger. 61 pp.
86. de Wolf, D. A. 1967. *J. Opt. Soc. Am.* 57: 1057–58
87. Disney, M. J. 1978. *Proc. ESO Conf. Opt. Telesc. of the Future*, ed. F. Pacini, W. Richter, R. N. Wilson, pp. 145–64. Geneva: ESO
88. Dommanget, J. 1963. *Proc. IAU Symp. No. 19, Site Testing*, pp. 235–49
89. Donelan, M., Miyake, M. 1973. *J. Atmos. Sci.* 30: 444–64
90. Downey, W. K., Stern, H., Wilson, K., Gibbs, S. 1981. In *Tech. Rep. 46*, Bur. Meteorol., Melbourne, Aust.
91. Duffieux, P. M. 1946. *L'Intégrale de Fourier et Ses Applications à l'Optique.* France: Besançon. 171 pp.
92. Dunn, R. B. 1969. *Sky Telesc.* 38: 368–75
93. Dyson, F. J. 1975. *J. Opt. Soc. Am.* 65: 551–58
94. Dyson, F. J. 1978. *Proc. ESO Conf. Opt. Telesc. of the Future*, pp. 439–44. Geneva: ESO
95. Elders, L. 1965. *Aristotle's Cosmology —A Comment on De Caelo.* Assen, Neth: Van Gorkum
96. Elias, P., Grey, D. S., Robinson, D. Z. 1952. *J. Opt. Soc. Am.* 42: 127–34
97. Engvold, O., Dunn, R. B., Livingston, W. C., Smartt, R. N. 1983. *Appl. Opt.* 22: 10–12
98. Fehrenbach, C., Bowen, I. S. 1966. In *Proc. IAU Symp. No. 27, The Construction of Large Telescopes*, pp. 165–75
99. Fellgett, P. B. 1979. *Proc. Int. Workshop on Image Process. in Astron.*, ed. G. Sedmak, M. Capaccioli, R. J. Allen, pp. 136–55. Trieste, Italy
100. Fried, D. L. 1965. *J. Opt. Soc. Am.* 55: 1427–35
101. Fried, D. L. 1966. *J. Opt. Soc. Am.* 56: 1372–79
102. Fried, D. L. 1976. *Proc. Soc. Photo-Opt. Instrum. Eng.* 75: 20–25
103. Fried, D. L. 1978. *J. Opt. Soc. Am.* 68: 1651–58
104. Fried, D. L. 1979. *Proc. IAU Colloq. No. 50, High Angular Resolution Stellar Interferometry*, pp. 26-1–24
105. Friehe, C. A., La Rue, J. C., Champagne, F. H., Gibson, C. H., Dreyer, G. F. 1975. *J. Opt. Soc. Am.* 65: 1502–11
106. Gascoigne, S. C. B. 1975. *Endeavour* 34: 131–35
107. Geiger, R. 1966. *The Climate Near the Ground.* Cambridge, Mass: Harvard Univ. Press. 611 pp.
108. Gezari, D., Labeyrie, A., Stachnik, R. 1971. *Bull. Am Astron. Soc.* 3: 244
109. Gillingham, P. R. 1978. *AAT Dome Seeing, A Progress Report.* Epping, NSW: Anglo-Aust. Obs. 31 pp.
110. Gillingham, P. R. 1981. *AAT Dome Seeing Progress Report.* Epping, NSW: Anglo-Aust. Obs. 27 pp.
111. Goodman, J. W. 1977. *Proc. IEEE* 65: 29–38
112. Goodman, J. W., Belsher, J. F. 1976. *Proc. Soc. Photo-Opt. Instrum. Eng.* 75: 141–54
113. Gracheva, M. E., Gurvich, A. S. 1965. *Sov. Radiophys.* 8: 511–15
114. Greenaway, A. H. 1980. *Proc. Conf. Opt. Infrared Telesc. for the 1990s*, pp. 755–85. Tucson: Kitt Peak Natl. Obs.
115. Grosso, R. P., Yellin, M. 1977. *J. Opt. Soc. Am.* 67: 399–406
116. Hall, D. N. B. 1967. *Appl. Opt.* 6: 1992–94
117. Hall, D. N. B. 1978. *Proc. ESO Conf. Opt. Telesc. of the Future*, ed. F. Pacini, W. Richter, R. N. Wilson, pp. 239–50. Geneva: ESO
118. Hanbury Brown, R. 1974. *The Intensity Interferometer.* London: Taylor & Francis. 183 pp.
119. Hanbury Brown, R. 1978. *Proc. ESO Conf. Opt. Telesc. of the Future*, ed. F. Pacini, W. Richter, R. N. Wilson, pp. 391–408. Geneva: ESO
120. Hanbury Brown, R. 1979. *Proc. IAU Colloq. No. 50, High Angular Resolution Stellar Interferometry*, pp. 11-1–17
121. Hanbury Brown, R. 1981. *Proc. Soc. Photo-Opt. Instrum. Eng.* 288: 545–50
122. Hanbury Brown, R., Twiss, R. Q. 1957. *Proc. R. Soc. London Ser. A* 242: 300–24
123. Hansen, R. T., Hansen, S. F. 1966. *Publ. Astron. Soc. Pac.* 78: 14–29
124. Hardy, J. W., Wallner, E. P. 1979. *Proc.*

IAU Colloq. No. 50, High Angular Resolution Stellar Interferometry, pp. 10-1–26
125. Hardy, J. W., Feinleib, J., Wyant, J. C. 1974. *Proc. Top. Meet. Opt. Propag. Through Turbul.*, pp. ThB1-1–4. Boulder: Univ. Colo
126. Hardy, J. W., Lefebre, J. E., Koliopoulos, C. L. 1977. *J. Opt. Soc. Am.* 67: 360–69
127. Harlan, E. A., Walker, M. F. 1965. *Publ. Astron. Soc. Pac.* 77: 246–52
128. Harris, J. L. 1966. *J. Opt. Soc. Am.* 56: 569–74
129. Hartley, M., McInnes, B., Smith, F. G. 1981. *Q. J. R. Astron. Soc.* 22: 272–78
130. Haugen, D. A., ed. 1973. *Proc. Workshop Micrometeorol.* Boston: Am. Meteorol. Soc. 392 pp.
131. Hawkins, M. R. F. 1979. *Astron. Astrophys.* 76: 46–49
132. Hoag, A. A. 1972. Private communication
133. Hogg, A. R. 1963. *Proc. IAU Symp. No. 19, Site Testing*, pp. 253–57
134. Hooke, R. 1665. *Micrographia, Observation LVIII.* Reprinted 1961, New York: Dover. 280 pp.
135. Hufnagel, R. E. 1966. *Proc. Woods Hole Summer Study*, Append. 5. Washington, DC
136. Hufnagel, R. E. 1974. In *Digest of Topical Meeting on Optical Propagation Through Turbulence*, ed. F. F. Hall, pp. WA1–4. Boulder: Univ. Colo
137. Hufnagel, R. E., Stanley, N. R. 1964. *J. Opt. Soc. Am.* 54: 52–60
138. Huiser, A. M. J. 1982. *Opt. Commun.* 42: 226–30
139. Jackson, P. S., Hunt, J. C. R. 1975. *Q. J. R. Meteorol. Soc.* 101: 929–55
140. Jakeman, E., Parry, G., Pike, E. R., Pusey, P. N. 1978. *Contemp. Phys.* 19: 127–46
141. Jefferies, J. T., Sinton, W. M. 1968. *Sky Telesc.* 36: 1–7
142. Jefferies, J. T., Zirker, J. B. 1966. *Preliminary Report on a Site for an 84-Inch Telescope, Univ. Hawaii Obs. Commun. No. 1.* 38 pp.
143. Kaimal, J. C. 1973. *Boundary-Layer Meteorol.* 4: 289–309
144. Kaimal, J. C., Eversole, R. A., Lenschow, D. H., Stankov, B. B., Kahn, P. H., Businger, J. A. 1982. *J. Atmos. Sci.* 39: 1098–1114
145. Kaimal, J. C., Wyngaard, J. C., Haugen, D. A., Coté, O. F., Izumi, Y., et al. 1976. *J. Atmos. Sci.* 33: 2152–69
146. Kallistratova, M. A., Timanovski, D. F. 1971. *Izv. Akad. Nauk SSSR, Atmos. Oceanic Phys.* 7: 46–48
147. Kiepenheuer, K. O. 1962. *Proc. Symp. Sol. Seeing, Rome, 1961*, pp. 49–54. Spoleto, Italy: Natl. Res. Counc.
148. Kiepenheuer, K. O., Schellenberger, W. 1973. *JOSO Rep. SIT 17*, Fraunhofer Inst., Freiburg, Fed. Repub. Ger.
149. Kiepenheuer, K. O., Schellenberger, W. 1974. *JOSO Rep. SIT 22*, Fraunhofer Inst., Freiburg, Fed. Repub. Ger. 10 pp.
150. Knox, K. T., Thompson, B. J. 1974. *Ap. J. Lett.* 193: L45–48
151. Kolmogorov, A. N. 1941. In *Turbulence*, pp. 151–55. Transl. S. K. Friedlander, L. Topper, 1961. New York: Interscience
152. Konrad, T. G. 1970. *J. Atmos. Sci.* 27: 1138–47
153. Korets, M. A., Ponizovskii, Z. L. 1976. *Priroda (Moscow)* 8: 22–27
154. Korff, D. 1973. *J. Opt. Soc. Am.* 63: 971–80
155. Krechmer, S. I. 1954. *Tr. Geofiz. Inst. Akad. Nauk SSSR* 24: 151–55
156. Kunkel, K. E., Walters, D. L. 1982. *Boundary-Layer Meteorol.* 22: 49–60
157. Labeyrie, A. 1970. *Astron. Astrophys.* 6: 85–87
158. Labeyrie, A. 1975. *Ap. J. Lett.* 196: L71–75
159. Labeyrie, A. 1978. *Proc. ESO Conf. Opt. Telesc. of the Future*, ed. F. Pacini, W. Richter, R. N. Wilson, pp. 375–86. Geneva: ESO
160. Lane, J. A. 1967. *Electron. Lett.* 3: 173–74
161. Lane, J. A. 1968. *Proc. Inst. Electr. Eng. (London)* 111: 275–83
162. Lawrence, R. S., Ochs, G. R., Clifford, S. F. 1970. *J. Opt. Soc. Am.* 60: 826–30
163. Lee, R. W., Harp, J. C. 1969. *Proc. IEEE* 57: 375–406
164. Léna, P. 1980. *Proc. Conf. Opt. Infrared Telesc. for the 1990s*, 2: 840–49. Tucson: Kitt Peak Natl. Obs.
165. Liewer, K. M. 1979. *Proc. IAU Colloq. No. 50, High Angular Resolution Stellar Interferometry*, pp. 8-1–14
166. Linfoot, E. H. 1964. *Fourier Methods in Optical Image Evaluation.* London: Focal. 90 pp.
167. Little, C. G. 1951. *MNRAS* 111: 289
168. Livingston, W. C., Harvey, J., Pierce, A. K., Schrage, D., Gillespie, B., et al. 1976. *Appl. Opt.* 15: 33–39
169. Loos, G. C., Hogge, C. B. 1979. *Appl. Opt.* 18: 2654–61
170. Loughhead, R. E., Bray, R. J., Tappere, E. J., Winter, J. G. 1968. *Sol. Phys.* 4: 185–95
171. Lüke, O. v. der 1981. *Astron. Astrophys.* 101: 277–83
172. Lumley, J. L., Panofsky, H. A. 1964. *The Structure of Atmospheric Turbulence.* New York: Interscience. 239 pp.

173. Lynds, C. R. 1960. *Physics of Seeing Program—Final Report on Initial Experimental Phase, Unnumbered Intern. Rep.*, Kitt Peak Natl. Obs., Tucson. 45 pp.
174. McGlamery, B. L. 1967. *J. Opt. Soc. Am.* 57:293–97
175. McInnes, B. 1981. *Q. J. R. Astron. Soc.* 22:266–71
176. McInnes, B., Walker, M. F. 1974. *Publ. Astron. Soc. Pac.* 86:529–44
177. McKnight, D. R., Jefferies, J. T. 1968. *A Site Survey of Mauna Kea—Meteorology, Inst. Astron. Rep.*, Univ. Hawaii, Honolulu. 35 pp.
178. Maltby, P. 1970. *JOSO Rep. MET 33*, Fraunhofer Inst., Freiburg, Fed. Rep. Ger.
179. Manton, M. J. 1977. *Boundary-Layer Meteorol.* 12:491–504
180. Mason, P. J., Sykes, R. I. 1979. *Q. J. R. Meteorol. Soc.* 105:383–95
181. Mast, T., Nelson, J. E. 1982. *Appl. Opt.* 21:2631–41
182. Mayfield, E. B., Vrabec, D., Rogers, E., Janssens, T., Becker, R. A. 1969. *Sky Telesc.* 37:208–13
183. Meinel, A. B. 1960. In *Telescopes*, ed. G. P. Kuiper, B. M. Middlehurst, pp. 154–75. Chicago: Univ. Chicago Press
184. Meinel, A. B. 1963. *Final Report of a Site Selection for a National Astronomical Observatory, Contrib. No. 45*, Kitt Peak Natl. Obs., Tucson, Ariz. 84 pp.
185. Meyer-Arendt, J. R., Emmanuel, C. B. 1965. *NBS Tech. Note No. 225*, Natl. Bur. Stand., Washington, DC. 140 pp.
186. Michelson, A. A., Pease, F. G. 1921. *Ap. J.* 53:249–59
187. Mikhel'son, N. N. 1976. *Opt. Mekh. Prom.* 43:62–65. Transl. in *Sov. J. Opt. Technol.* 43:446–49
188. Miller, M. G., Kellen, P. F. 1975. *Proc. Top. Meet. Imaging Astron.*, pp. WB3-1–4. Cambridge, Mass: Opt. Soc. Am.
189. Miller, L., Brown, W. P., Jenney, J. A., O'Meara, T. R. 1974. *Proc. Top. Meet. Opt. Propag. Through Turbul.*, pp. ThB2-1–4. Boulder: Univ. Colo
190. Miyake, M., Stewart, R. W., Burling, R. W. 1970. *Q. J. R. Meteorol. Soc.* 96:138–43
191. Mizuno, T., Panofsky, H. A. 1975. *Boundary-Layer Meteorol.* 9:375–80
192. Monin, A. S., Yaglom, A. M. 1971. *Statistical Fluid Mechanics*, Vol. 1. Cambridge, Mass: MIT Press. 769 pp.
193. Monin, A. S., Yaglom, A. M. 1975. *Statistical Fluid Mechanics*, Vol. 2. Cambridge, Mass: MIT Press. 874 pp.
194. Moroder, E., Righini, A. 1973. *Astron. Astrophys.* 23:307–10
195. Morrison, D., Murphy, R.-E., Cruikshank, D. P., Sinton, W. M., Martin, T. Z. 1973. *Publ. Astron. Soc. Pac.* 85:255–67
196. Muller, R. 1973. *Sol. Phys.* 32:409–20
197. Muller, R. A., Buffington, A. 1974. *J. Opt. Soc. Am.* 64:1200–10
198. Munn, R. E. 1966. *Descriptive Micrometeorology*. New York: Academic. 245 pp.
199. Murdin, P., Bingham, R. G. 1975. *Observatory* 95:180–87
200. National Research Council of Italy. 1962. *Proc. Symp. Sol. Seeing, Rome, 1961*. 158 pp.
201. Neff, W. D. 1975. *NOAA Tech. Rep. ERL 322-WPL 38*, Wave Propag. Lab., Boulder, Colo. 34 pp.
202. Nettleblad, F. 1953. *Lund Obs. Medd. Ser. 2* 130:1–98
203. Newton, I. 1730. *Opticks*, Bk. 1, Pt. 1, Prop. 8. Reprinted 1952, New York: Dover. 406 pp.
204. Nieuwstadt, F. T. M., Driedonks, A. G. M. 1979. *J. Appl. Meteorol.* 18:1397–1405
205. Obukhov, A. M. 1946. *Tr. Inst. Teor. Geofiz. Akad. Nauk USSR* 1:95
206. Ochs, G. R., Lawrence, R. S. 1972. *NOAA Tech. Rep. ERL 251-WPL 22*, Wave Propag. Lab., Boulder, Colo. 40 pp.
207. Ochs, G. R., Wang, T.-I., Lawrence, R. S., Clifford, S. F. 1976. *Appl. Opt.* 15:2504–10
208. Pearlman, M. R., Bufton, J. L., Hogan, D., Kurtenbach, D., Goodwin, K. 1974. *SAO/NASA Spec. Rep. No. 357*, Smithsonian Astrophys. Obs., Cambridge, Mass. 82 pp.
209. Pearlman, M. R., Hogan, D., Kirchhoff, W., Goodwin, K., Kurtenbach, D. 1970. *Spec. Rep. No. 327*, Smithsonian Astrophys. Obs., Cambridge, Mass. 34 pp.
210. Pearson, J. E. 1981. *Laser Focus* 17:53–61
211. Pearson, J. E., Bridges, W. S., Horwitz, L. S., Ogrodnik, R. F. 1974. *Proc. Top. Meet. Opt. Propag. Through Turbul.*, pp. ThB5-1–3. Boulder: Univ. Colo
212. Perrin, F. H. 1960. *J. SMPTE* 69:151–56
213. Perrin, F. H. 1960. *J. SMPTE* 69:239–49
214. Priestley, C. H. B. 1959. *Turbulent Transfer in the Lower Atmosphere*. Chicago: Univ. Chicago Press. 130 pp.
215. Protheroe, W. M., Chen, K. Y. 1960. *Air Force Cambridge Res. Cent. Tech. Rep. AF19(604)-1570*, Geophys. Res. Dir., Bedford, Mass. 81 pp.
216. Queney, P., Corby, G. A., Gerbier, N.,

Koschmieder, H., Zierep, J. 1960. *WMO Tech. Note No. 34.* 135 pp.
217. Ramsay, J. V. 1959. *Opt. Acta* 6: 344–53
218. Ramsay, J. V., Kobler, H. 1962. *Observatory* 82: 107–11
219. Rayment, R., Readings, C. J. 1974. *Q. J. R. Meteorol. Soc.* 100: 221–33
220. Reiger, S. H. 1963. *Astron. J.* 68: 395–406
221. Ricort, G., Aime, C. 1979. *Astron. Astrophys.* 76: 324–35
222. Rocca, A., Roddier, F., Vernin, J. 1974. *J. Opt. Soc. Am.* 64: 1000-4
223. Roddier, F. 1981. *Prog. Opt.* 19: 283–368
224. Roddier, C., Roddier, F. 1973. *J. Opt. Soc. Am.* 63: 661–63
225. Roll, H. V. 1965. *Physics of the Marine Atmosphere.* New York: Academic. 426 pp.
226. Rösch, J. 1956. *Proc. Symp. Astron. Opt.*, ed. Z. Kopal, pp. 310–17. Amsterdam: North-Holland
227. Rösch, J. 1957. *C. R. Acad. Sci. Paris* 244: 3027–30
228. Rösch, J. 1962. *Proc. Symp. Sol. Seeing, Rome, 1961,* pp. 35–48. Spoleto, Italy: Natl. Res. Counc.
229. Rösch, J., Courtès, G., Dommanget, J., eds. 1963. *Proc. IAU Symp. No. 19, Site Testing.* 382 pp.
230. Rytov, S. M. 1937. *Izv. Akad. Nauk SSR Ser. Fiz.* 2: 223–59
231. Safronov, A. N. 1981. *Avtometriia* 2: 13–17
232. Shawcross, W. E., ed. 1977. *Sky Telesc.* 53: 254–56
233. Smith, F. D. 1963. *Appl. Opt.* 2: 335–50
234. Smith, F. G. 1981. *Q. J. R. Astron. Soc.* 22: 254–65
235. Smith, R. B. 1979. *Adv. Geophys.* 21: 87–217
236. Stock, J. 1963. *Proc. IAU Symp. No. 19, Site Testing,* pp. 249–53
237. Stock, J., Keller, G. 1960. In *Telescopes,* ed. G. P. Kuiper, B. M. Middlehurst, pp. 138–53. Chicago: Univ. Chicago Press
238. Strittmatter, P. A. 1978. *Proc. ESO Conf. Opt. Telesc. of the Future,* ed. F. Pacini, W. Richter, R. N. Wilson, pp. 165–84. Geneva: ESO
239. Strobehn, J. W. 1968. *Proc. IEEE* 56: 1301–18
240. Strobehn, J. W. 1978. *Top. Appl. Phys.* 25: 45–104
241. Sutton, O. G. 1953. *Micrometeorology.* New York: McGraw-Hill. 333 pp.
242. Tango, W. J. 1979. *Proc. IAU Colloq. No. 50, High Angular Resolution Stellar Interferometry,* pp. 13-1–7
243. Tatarski, V. I. 1959. *Wave Propagation in a Turbulent Medium.* Transl. R. Silverman, 1961. New York: McGraw-Hill. 285 pp.
244. Tatarski, V. I. 1967. *The Effects of the Turbulent Atmosphere on Wave Propagation.* Transl. J. W. Strobehn, 1971. Jerusalem: Isr. Program Sci. Transl. 472 pp.
245. Tatarski, V. I., Gurvich, A. S., Elepov, B. S., Pokasov, V. V., Sabelfeld, K. K. 1979. *Opt. Acta* 26: 531–42
246. Taylor, G. I. 1935. Republished 1961 in *Turbulence,* ed. S. K. Friedlander, L. Topper, pp. 18–75. New York: Interscience
247. Taylor, R. J. 1958. *Aust. J. Phys.* 11: 168–74
248. Thomas, D. V., Perry, J. E. 1976. *Royal Greenwich Observatory Rep. for January–September 1975.* 55 pp.
249. Thomas, D. V., Perry, J. E. 1977. *Royal Greenwich Observatory Rep. for 1975–76.* 64 pp.
250. Tokovinin, A. A., Shcheglov, P. V. 1979. *Sov. Phys.-Usp.* 22: 960–74
251. Trabka, E. 1966. *J. Opt. Soc. Am.* 56: 128–29
252. Tsvang, L. R. 1969. *Radio Sci.* 4: 1175–77
253. Tuzet, A. 1982. Thesis No. 688. Univ. Clermont II, Fr. 71 pp.
254. Tuzet, A., Guillemet, B., Isaka, H. 1982. *J. Rech. Atmos.* 17: 185–97
255. Valley, G. C. 1979. *Appl. Opt.* 18: 984–87
256. Vernin, J., Roddier, F. 1973. *J. Opt. Soc. Am.* 63: 270–73
257. Walker, M. F. 1970. *Publ. Astron. Soc. Pac.* 82: 672–98
258. Walker, M. F. 1971. *Publ. Astron. Soc. Pac.* 83: 401–22
259. Walker, J. G. 1982. *Appl. Opt.* 21: 3132–37
260. Walters, D. L. 1981. *J. Opt. Soc. Am.* 71: 406–9
261. Walters, D. L., Kunkel, K. E. 1981. *J. Opt. Soc. Am.* 71: 397–405
262. Walters, D. L., Favier, D. L., Hines, J. R. 1979. *J. Opt. Soc. Am.* 69: 828–37
263. Warner, J. 1972. *Q. J. R. Meteorol. Soc.* 98: 175–86
264. Warner, J. 1973. *Q. J. R. Meteorol. Soc.* 99: 82–88
265. Webb, E. K. 1964. *Appl. Opt.* 3: 1329–36
266. Wesely, M. L. 1976. *J. Appl. Meteorol.* 15: 43–49
267. Wesely, M. L., Hicks, B. B. 1978. *J. Appl. Meteorol.* 17: 123–28
268. Whitford, A. E., Stebbins, J. 1936. *Publ. Am. Astron. Soc.* 8: 228
269. Woolf, N. J. 1982. *Ann. Rev. Astron. Astrophys.* 20: 367–98
270. Wyngaard, J. C. 1975. *Boundary-Layer Meteorol.* 9: 441–60

271. Wyngaard, J. C., Coté, O. R. 1971. *J. Atmos. Sci.* 28:190–201
272. Wyngaard, J. C., Le Mone, M. A. 1980. *J. Atmos. Sci.* 37:1573–85
273. Wyngaard, J. C., Izumi, Y., Collins, S. A. 1971. *J. Opt. Soc. Am.* 61:1646–50
274. Wyngaard, J. C., Pennell, W. T., Lenschow, D. H., Le Mone, M. A. 1978. *J. Atmos. Sci.* 35:47–58
275. Yaglom, A. M. 1962. *Theory of Stationary Random Functions.* Transl. R. Silverman. Englewood Cliffs, NJ: Prentice-Hall. 235 pp.
276. Yamada, T. 1979. *J. Appl. Meteorol.* 18:526–31
277. Young, A. T. 1969. *Appl. Opt.* 8:869–85
278. Young, A. T. 1974. *Ap. J.* 189:587–604
279. Zubkovski, S. L., Kravchenko, T. K. 1967. *Izv. Akad. Nauk SSSR, Atmos. Oceanic Phys.* 3:170–91

Annual Review of Astronomy and Astrophysics
Volume 23, 1985

CONTENTS